Direct Observation of Metal-to-Ligand Charge-Transfer (MLCT) Excited States of Pentaammineruthenium(II) Complexes

Jay R. Winkler,* Thomas L. Netzel,*† Carol Creutz,* and Norman Sutin*

Contribution from the Department of Chemistry, Brookhaven National Laboratory, Upton, New York 11973. *Received June 26, 1986*

Abstract: Excited-state difference spectra and lifetimes are reported for $Ru(tpy)_2^{2+}$ (tpy = 2,2′,2″-terpyridine) and a series of pentaammineruthenium(II) complexes. The initially formed excited states (generated by ~25-ps excitation with 532-nm light) are well modeled by a $Ru^{III}(L^{\bullet-})$ electronic configuration (L is an aromatic, N-heterocycle ligand) since an excellent correspondence is found between their absorption features and those of $(L^{\bullet-})H^+$ radicals. The transients are, therefore, assigned as MLCT states. The $Ru(tpy)_2^{2+}$ excited-state lifetime is 250 ps. The $Ru(NH_3)_5L^{2+}$ excited-state lifetimes vary from ≤20 (L = protonated pyrazine, protonated 4,4′-bipyridine, and 4-acetylpyridine) to ~200 (L = pyrazine, isonicotinamide, 4,4′-bipyridine) ps in water at ~22 °C. Ammine aquation products, $Ru(NH_3)_4(H_2O)L^{2+}$, are also observed and are shown to result from multiphoton absorption of the ps-excitation pulses. The MLCT states of $Ru(NH_3)_5L^{2+}$ (L = pz or 4,4′-bpy) undergo protonation by solvent water and deactivation to $Ru(NH_3)_5LH^{3+}$; rate constants for proton loss from the protonated species ($Ru(NH_3)_5LH^{3+} + H_2O \rightarrow Ru(NH_3)_5L^{2+} + H_3O^+$) are (2–3) × 10^7 s^{-1} and 2 × 10^5 s^{-1} for L = pz and 4,4′-bpy, respectively. The $Ru(NH_3)_5L^{2+}$ MLCT-excited-state lifetimes are discussed in terms of the lowest excited state tuning model of Ford and co-workers.

Pentaammineruthenium(II) complexes with aromatic N-heterocyclic ligands (L) provide a fruitful field for the study of inorganic photochemical reaction mechanisms.[1] They also provide the building blocks for the binuclear complexes which have been the subject of intramolecular electron-transfer studies.[2] Furthermore, the excited-state manifolds in the pentaammineruthenium(II) series are related to those of the much studied poly(pyridine)ruthenium(II) complexes.[3]

The visible spectra of $Ru(NH_3)_5L^{2+}$ are dominated by intense metal-to-ligand charge-transfer (MLCT) bands[4] which are both L and solvent dependent,[4,5] but irradiation of $Ru(NH_3)_5L^{2+}$ with visible light leads to photosubstitution processes characteristic of ligand-field photochemistry.[1] Detailed photochemical studies of the pentaammineruthenium(II) complexes began in the late 1960's and culiminated in the "excited-state tuning" model about 10 years later.[6] The most striking photochemical observation was the dramatic decrease in photoaquation yield that occurred when the MLCT band of these complexes was shifted to the red by variation of the heterocyclic amine (L). The $Ru(NH_3)_5L^{2+}$ complexes with MLCT absorption maxima ≤460 nm were found to have large photoaquation quantum yields that were independent of the irradiation wavelength. By contrast, $Ru(NH_3)_5L^{2+}$ complexes with MLCT absorption maxima at longer wavelengths had wavelength-dependent quantum yields for photoaquation.[6c]

Thermal substitution inertness characterizes both Ru(II)– and Ru(III)–ammine complexes. Thus there is no reason to expect a MLCT excited state of a $Ru(NH_3)_5L^{2+}$ complex to undergo facile ligand substitution. Population of a metal–ligand antibonding orbital, as in the lowest energy ligand-field transition $^1A_{1g}(t_{2g}^6) \rightarrow {}^{1,3}T_{1g}(t_{2g}^5e_g^1)$ in O_h symmetry, however, should render a ruthenium–ammine complex substitution labile. The "excited state tuning" model accounts for the quantum yield observations in a manner consistent with the above MLCT and LF labilization expectations.[6c] In this model, complexes with MLCT absorption maxima ≤460 nm are viewed as having lowest energy excited states (LEES) that are ligand-field in character. Complexes with MLCT absorption maxima >460 nm are viewed as having LEES that are MLCT in character. The model has proven qualitatively useful but a lack of spectroscopic and photophysical data have precluded quantitative modeling. While Cremers has observed emission from some $Ru(NH_3)_5L^{2+}$ solids at 77 K,[7] considerable uncertainty remains regarding the locations of the (0,0) levels of the lowest energy MLCT and LF states in these complexes.

In the present work we have utilized picosecond absorption spectroscopy to measure the spectra of the primary MLCT excited states and find that these are consistent with those expected from a model of these states as $Ru^{III}L^{\bullet-}$ species. We also report electrochemical and spectral data and photoaquation yields for several complexes under continuous and picosecond photolysis conditions. In addition, a detailed model for the photophysical manifolds of these complexes is considered.

Experimental Procedures

Kinetics and Spectral Measurements. Figure 1 is a schematic representation of the mode-locked Nd/YAG laser system (Korad KY40 with Quantel amplifiers) used to measure difference spectra, kinetics, and emission lifetimes. The ~30-ps pulses at 1064 nm are generated in an actively–passively mode-locked oscillator cavity. A Pockels cell (Quantel SPS411 Pulse Selector) with crossed polarizers is positioned between the oscillator and first amplifier to select a single pulse from the train of mode-locked pulses. The repetition rate of the laser system is one firing per second. A spatial filter is placed between the first two amplifiers. It consists of a near-field aperture, a 2.4-m radius reflector, a pinhole aperture, and a 2-m focal-length collimating lens. A 1.5:1 beam expander is located after the second amplifier.

Eighty percent of the output of the first two amplifiers is sent to a translation stage with mirrors 90° apart. In most of the experiments described in this paper, a second-harmonic-generating KDP crystal was inserted into the laser beam before the delay line in order to generate probe light with 532-nm pulses (by focussing into a 10-cm cell containing D_2O and H_2O, 80:20 by volume). The instrument reponse under these conditions is 20–25 ps. For some experiments the probe light was generated with 1064-nm pulses producing an instrument response of 30–35 ps. Although the probe-light wavelength range is greater than 360–850 nm, the photomultipliers used (Hamamatsu R928) are too insensitive for measurements above 850 nm and the achromatic lenses absorb strongly below 360 nm. The probe light is collected and focussed onto a 400-

† Present address: Amoco Corporation, Amoco Research Center, Post Office Box 400 (F-6), Naperville, IL 60566.

(1) (a) Ford, P. C.; Wink, D.; DiBenedetto, T., *Prog. Inorg. Chem.* **1983**, *30*, 213. (b) Ford, P. C. *Coord. Chem. Rev.* **1982**, *44*, 61.
(2) (a) Schanze, K. S.; Meyer, T. J. *Inorg. Chem.* **1985**, *24*, 2121. (b) Creutz, C.; Kroger, P.; Matsubara, T.; Netzel, T. L.; Sutin, N. *J. Am. Chem. Soc.* **1979**, *101*, 5442.
(3) See: Kalyanasundaram, K. *Coord. Chem. Rev.* **1982**, *46*, 159.
(4) Ford, P. C.; Rudd, De F. P.; Gaunder, R.; Taube, H. *J. Am. Chem. Soc.* **1968**, *90*, 1187.
(5) Curtis, J. C.; Sullivan, B. P.; Meyer, T. J. *Inorg. Chem.* **1983**, *22*, 224.
(6) (a) Ford, P. C. *Coord. Chem. Rev.* **1970**, *5*, 75. (b) Chaisson, D. A.; Hintze, R. E.; Stuermer, D. H.; Petersen, J. D.; McDonald, D. P.; Ford, P. C. *J. Am. Chem. Soc.* **1972**, *94*, 6665. (c) Malouf, D.; Ford, P. C. *J. Am. Chem. Soc.* **1977**, *99*, 7213. (d) Durante, V. A.; Ford, P. C. *Inorg. Chem.* **1979**, *18*, 588.
(7) Cremers, T. L. Ph.D. Thesis, 1980, Washington State University.

0002-7863/87/1509-2381$01.50/0

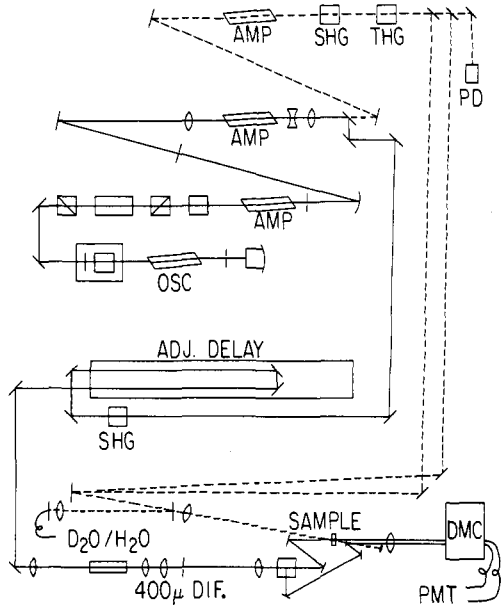

Figure 1. Picosecond transient absorption spectrometer: OSC, Nd:YAG oscillator; AMP, Nd:YAG laser amplifier; SHG and THG, second and third harmonic generating crystals, respectively; PD, photodiode for triggering detection circuitry; ADJ DELAY, translation stage with 2 m of travel; D_2O/H_2O, 10 cm path length cell containing a mixture of D_2O and H_2O (80:20 by volume); 400 μ DIF., 400-μm aperture in contact with a glass diffuser; SAMPLE, 2 mm path length cell; DMC, double $^1/_4$ m monochromator; PMT, photomultiplier tubes.

μm-diameter aperture in contact with a sand-blasted glass slide. This apertured scatter-plate homogenizes the wavelength distribution in space, depolarizes the probe light, and defines a point source of light for subsequent imaging. As a result, movements of the laser beam caused by translating the delay stage are decoupled from the imaging system that transfers the probe light from the scatter-plate through the sample to the detectors. Such beam movements can alter the intensity of the probe light transmitted through the scatter-plate, but they do not affect the locations of any scatter-plate images. Consequently, the overlap of the probe and excitation beams in the sample and the transmission of the probe light through the double monochromator are invariant with respect to the translation stage position.

An image of the scatter plate is relayed (1:1) to the sample with a 36-cm lens (f/15 collection efficiency). A large f-number relay-lens was chosen because smaller f-number lens choices did not form sharp images in the sample-cell region. One-third of the probe light is reflected around the sample to form a reference beam. The probe and reference beams are realigned with a 3-mm separation after the sample and relayed (1:1) into the entrance slit of the DMC (Spex $^1/_4$-m double monochromator in additive dispersion, 1200-grooves/mm gratings). The band-pass, determined by the 1-mm-diameter optical fibers at the exit of the DMC, is 1.9 nm. This light is transported via optical fibers to two photomultipliers where the photocurrent is amplified, shaped, and sent to sample-and-hold and ADC circuitry. The digitized voltages proportional to the light in each probe beam are processed in a PDP 11/23 CPU. For each measurement at a specified delay time and wavelength, 100 laser firings are used. Fifty ratios of the two beams are measured *without* photoexcitation of the sample and fifty ratios are measured *with* sample excitation. The log of the ratio of these ratios yields a ΔA (absorbance change) value. The standard deviation of the mean of these ΔA values is the reported precision of the measurements. Although increased averaging can reduce the statistical error of each ΔA measurement, the present precision is a good estimate of the accuracy of each measurement. Sample decomposition or other changes (e.g., dust or film accumulation) make it unlikely that more precise measurements would be more accurate. The present accuracy of this system is ± 0.001 ΔA for the most stable samples. Measurements in the near-UV and near-IR have larger errors due solely to the poorer photon-statistics of the probe beams in these regions.

Twenty percent of the output of the first two laser amplifiers is coupled into a third amplifier having a 9-mm-diameter laser rod. This beam of 1064-nm light is used to generate the photoexcitation wavelengths. In this paper both the second harmonic at 532 nm and the third harmonic at 355 nm were used. The photodiode behind the harmonic-generating crystals provides a trigger pulse to initiate the A-to-D conversions. The dashed lines in Figure 1 show the paths of the excitation beams from the third amplifier to the sample. For 532-nm excitation the THG crystal and the following mirror are removed. To reject 532-nm light in the 355-nm beam, a dielectric reflector ($R > 99.9\%$ at 532 nm) is placed in the UV light path. Finally, a beam splitter in the excitation beam before the 1 m focal length lens directs a few percent of this light into an optical fiber. This signal is recorded for each laser shot. Data from excitation pulses outside a preselected energy range are rejected.

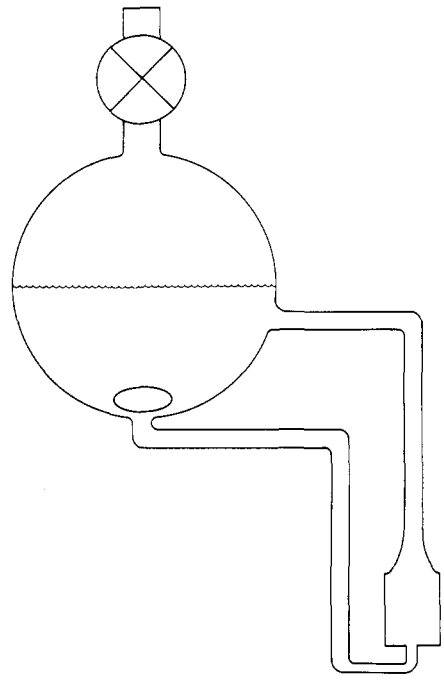

Figure 2. The all-glass flow cell for the picosecond experiments.

The above laser system separates the control of the probe-light generation from the control of the excitation-pulse energy. This design facilitates energy-dependence studies since the excitation energy can be independently adjusted by changing the voltage or timing settings of the third amplifier. Such studies are important because many inorganic and organometallic systems produce multiphoton "artifacts" at easily attainable excitation energies ($\gtrsim$1 mJ/pulse). Indeed the avoidance of such artifacts is a strong argument for using the maximum possible excitation repetition rate. Our present 1 Hz repetition rate is nearly the minimum acceptable rate.

The samples were held at room temperature under argon in the all-glass flow cell shown in Figure 2. The main reservoir was magnetically stirred to create regions of high and low velocity. A 2 mm path length sample cell inserted into this transfer line ensured that each measurement would be made on a fresh sample. The vertical flow rate in the sample cell was about 2 cm/s. The photoexcitation and probe beams crossed at a small angle in the sample cell. The position of the 1 m focal length lens in the excitation beam was chosen so that the diameter of the photoexcitation beam in the center of the sample cell was three to four times the diameter of the probe beam. This geometry enabled absorbance changes in the range 1.0–0.001 to be measured.

To extend the observation time range while maintaining ps excitation, the ps continuum interrogation source was replaced with a pulsed (1–4 ms) or CW xenon lamp. A transient digitizer (LeCroy TR8828B) was connected to the output of a five-stage photomultiplier tube whose signal was preprocessed by a 200 MHz bandwidth, quasidifferential amplifier. With these changes, transients can be monitored over the 10^{-8} to 1 s time range. A full description of this system has been given elsewhere.[8]

Under "low power" conditions laser excitation energies were typically 0.8 mJ per pulse at 532 nm, giving a photoexcitation intensity in the sample of $\sim 7 \times 10^3$ einsteins cm^{-2} s^{-1} assuming a 25 ps rectangular pulse. The irradiated volume is estimated to be ~ 4 μL.

Quantum Yields. The irradiation sources for continuous photolysis experiments were a 450-W Xe lamp for visible excitation and a 500-W Hg lamp for UV excitation (Christie Electric Corp.). The collimated lamp output passed through a water filter to remove IR radiation, through cutoff filters to remove higher energy light, then finally through a narrow bandpass interference filter (fwhm $\approx$ 5 nm). The excitation

(8) Winkler, J. R.; Nocera, D. G.; Netzel, T. L. *J. Am. Chem. Soc.* **1986**, *108*, 4451.

wavelengths for $Ru(NH_3)_5(4,4'\text{-bpy})^{2+}$ and $Ru(NH_3)_5(4,4'\text{-bpyH})^{3+}$ were 500 and 560 nm, respectively. The light intensity (typically 3×10^{-8} einstein cm^{-2} s^{-1} for the visible) was determined with a calibrated thermopile (Eppley Laboratory, Inc.).[9]

The quantum yield for ammonia loss from $Ru(NH_3)_5(4,4'\text{-bpy})^{2+}$ was determined as follows. Two 14-mL solutions of 0.01 M pH 7 sodium phosphate buffer were deaerated with an Ar purge for 2 h and then transferred under Ar in the dark onto 6–7-mg samples of $[Ru(NH_3)_5(4,4'\text{-bpy})]Cl_2$ and purged for 15 min more. One solution was transferred under Ar into a 5-cm photolysis cell, purged for 5 min more, and then sealed by stopcock. The other solution was then sealed off and kept in the dark. The concentration of $Ru(NH_3)_5(4,4'\text{-bpy})^{2+}$ ($\sim$1 mM) was sufficient to completely absorb the excitation light. The sample was irradiated with approximately 1 equiv of photons (λ_{ex} = 500 nm, $t \approx 10$ min) while being vigorously stirred. Then both irradiated and dark samples were loaded onto 2 × 1 cm Sephadex C-25 cation exchange columns that had been equilibrated with 0.01 M NaCl. The columns were eluted with 0.33 M NaCl, and 5-mL fractions were collected until the color of the ruthenium complex appeared in the eluate. The fractions were analyzed for ammonia with an Orion Research ammonia electrode (Model 95-10) calibrated against a series of standard aqueous (10^{-5} to 10^{-3} M) NH_4Cl solutions. The ammonia yields (Y = moles of NH_3/moles of Ru) in the "dark" solution were typically 10–25% as great as in the photolyzed solution. Quantum yields for NH_3 loss were calculated from $\phi_{NH_3} = [Y_P - Y_T]N/P$, where P is the number of einsteins of photons absorbed, Y_P is the NH_3 yield in the irradiated sample, Y_T is the NH_3 yield in the dark sample, and N is the moles of complex in the photolyzed solution. In control experiments, ammonia collection efficiencies were found to be greater than 95%.

An analogous procedure was used for $Ru(NH_3)_5(4,4'\text{-bpyH})^{3+}$. The solvent used was 0.1 M aqueous HCl, the cation exchange column was equilibrated with 0.1 M HCl, and the column was eluted with 0.33 M HCl.

Ammonia yields resulting from picosecond laser photolysis of 50 mL of a 5×10^{-4} M $Ru(NH_3)_5(4,4'\text{-bpy})^{2+}$ solution were determined by an analogous procedure of cation exchan[illegible] chromatography followed by ammonia electrode analysis.

Sample Preparation. The complexes $[Ru(NH_3)_5L]X_2$ [L = pyridine (py), pyrazine (pz), isonicotinamide (isn), 4-acetylpyridine (4-acpy), 4,4'-bipyridine (4,4'-bpy); X = PF_6^-, ClO_4^-, $CF_3SO_3^-$] and $[Ru(tpy)_2](ClO_4)_2$ (tpy = 2,2',2''-terpyridine) were prepared according to published procedures.[4,10,11] All compounds were characterized by their electronic absorption spectra.

Water was purified by passing house-distilled water through a Millipore Q3 water-purification system. Acetonitrile (Burdick and Jackson) was dried 3 days under vacuum over activated alumina and then transferred and stored under vacuum over activated 3 Å molecular sieves. Aqueous solutions used in the picosecond spectroscopic experiments (typically, 50 mL) were deoxygenated with an Ar purge for at least 1 h, transferred under Ar to the flowcell, and stirred for another 30 min to 1 h under a stream of Ar. The flowcells were sealed with rubber septa under a slight positive pressure of Ar. Samples in nonaqueous solutions were prepared by flask-to-flask distillation of solvent ($\sim$50 mL) directly into the flowcell on a high-vacuum line ($<10^{-5}$ Torr). Solutions were further degassed with at least 3 freeze–pump–thaw cycles and then blanketed with a slight positive pressure of Ar and sealed with a high-vacuum Teflon stopcock. Absorption spectra of the samples were measured directly in the flowcells before and after data collection. Sample concentrations were in the 1–5 × 10^{-4} M range and are noted in the figure captions.

Results

$Ru(tpy)_2^{2+}$. Figure 3 shows spectral and kinetics results for $Ru(tpy)_2^{2+}$ in water after excitation with a $\sim$20-ps pulse at 532 nm. The kinetics were monitored at 470 nm, and the difference spectrum was recorded 50 ps (circles) and 11.5 ns (triangles) after photoexcitation. The t = 50 ps spectrum is characterized by bleaching of the ground-state absorption at 480 nm and absorbance increases to the blue and to the red of this band. The strong absorbance increase at 360 nm is characteristic of a polypyridine MLCT state[12] (see below) and arises from absorptions due to a reduced polypyridine ligand, $Ru^{III}(tpy)(tpy^{\bullet-})^{2+}$. The t = 11.5 ns measurements at 400, 450, and 500 nm indicate that ground-state repopulation is complete at this time. The 470-nm data show that ground-state repopulation follows first-order kinetics with a (1/e) lifetime of 250 ps (shorter than previously estimated by indirect methods[11,13]). No significance can be attached to the non-zero asymptote for the nonlinear least-squares fit to the data: $\Delta A(t \rightarrow \infty)$ is "zero" within experimental error. The emission yield is estimated[14] as $<10^{-5}$ in water at 295 K.

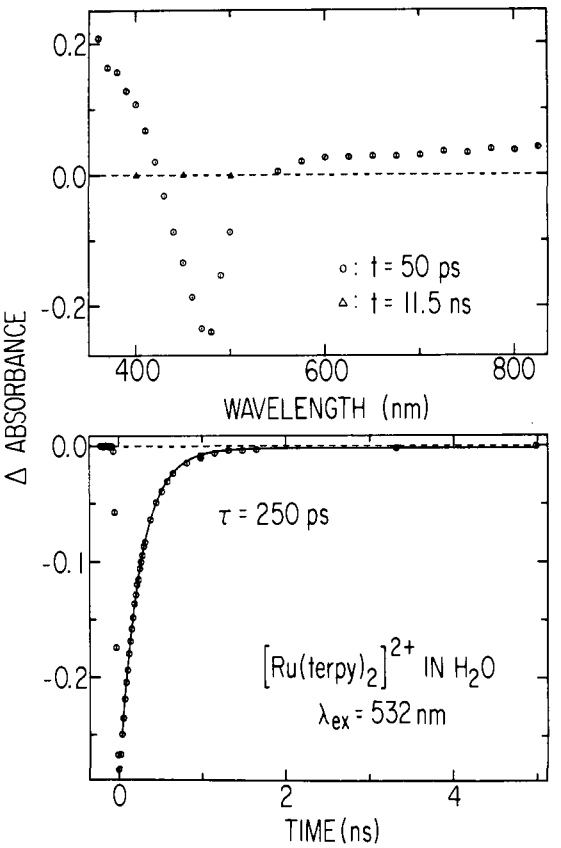

Figure 3. Transient difference spectra and kinetics for $[Ru(2,2',2''\text{-terpy})_2](ClO_4)_2$ in H_2O (3×10^{-4} M). Upper: difference spectra recorded 50 ps (O) and 11.5 ns (Δ) after 532-nm laser excitation. Lower: kinetics recorded at 470 nm; solid curve is a single exponential decay function with rate constant $k = 4 \times 10^9$ s^{-1}.

Table I. Reduction Potentials for Pentaammineruthenium Complexes in Acetonitrile vs. Aqueous SCE (0.1 M Tetraethylammonium Perchlorate Electrolyte)[a]

ligand, L	$E_{1/2}$, V, $Ru(NH_3)_5L$ Ru(III)/Ru(II)	L/L^-	$E_{1/2}$, V L/L^-
py	+0.36[d]	*b*	−2.69[e]
pz	+0.46	*b*	−2.11[e]
4,4'-bpy	+0.33	−1.83[c]	−1.85[e]
2,2'-bpy	+0.52	−1.77	−2.13[e]
$4,4'\text{-bpyCH}_3^+$	+0.36	−0.95	−1.03
$4,4'\text{-bpyH}^+$	+0.36	−0.88	
$pzCH_3^+$	+0.88	−0.76	−0.73[e]

[a] The $E_{1/2}$ values are taken as the average of the cathodic and anodic peak potentials. [b] For L = py, pz, isn the L/L^- process was beyond the solvent range (<−2 V). [c] Anodic wave detected only at v = 500 mV/s. [d] From ref 5. [e] Wiberg, K. B.; Lewis, T. P. *J. Am. Chem. Soc.* **1970**, *92*, 7154.

(9) Ghosh, P. K.; Brunschwig, B. S.; Chou, M.; Creutz, C.; Sutin, N. *J. Am. Chem. Soc.* **1984**, *106*, 4772.
(10) Lavallee, D. K.; Fleischer, E. B. *J. Am. Chem. Soc.* **1972**, *94*, 2583.
(11) Lin, C. T.; Böttcher, W.; Chou, M.; Creutz, C.; Sutin, N. *J. Am. Chem. Soc.* **1976**, *98*, 6536.
(12) Creutz, C.; Chou, M.; Netzel, T. L.; Okumura, M.; Sutin, N. *J. Am. Chem. Soc.* **1980**, *102*, 1309.
(13) Young, R. C.; Nagle, J. K.; Meyer, T. J.; Whitten, D. G. *J. Am. Chem. Soc.* **1978**, *100*, 4773.
(14) This estimate is based on τ = 250 ps for $Ru(tpy)_2^{2+}$ and the assumption of identical radiative rate constants for the luminescent states of $Ru(tpy)_2^{2+}$ and $Ru(bpy)_3^{2+}$ (see: Demas, J. N.; Crosby, G. A. *J. Am. Chem. Soc.* **1971**, *93*, 2841; van Houten, J.; Watts, R. J. *J. Am. Chem. Soc*, **1976**, *98*, 4853).

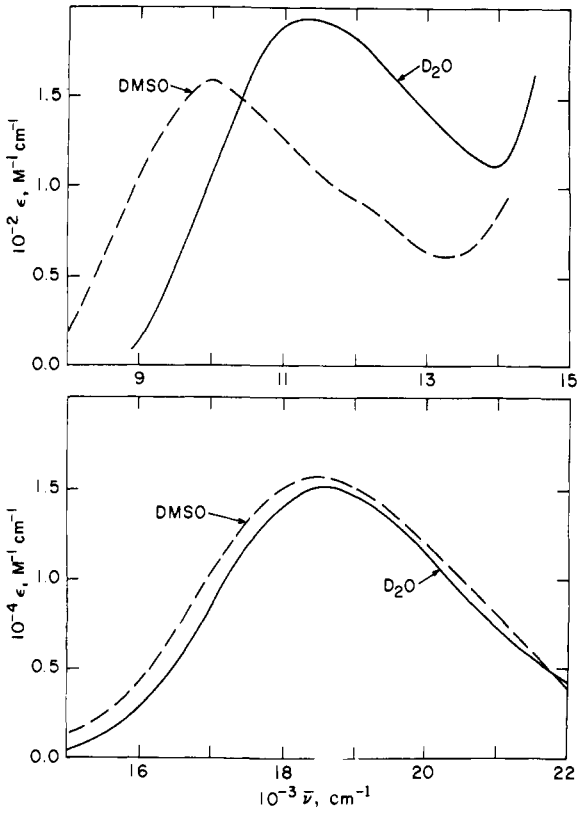

Figure 4. Ground-state spectra of $Ru(NH_3)_5(pzCH_3)^{3+}$ in water and dimethyl sulfoxide.

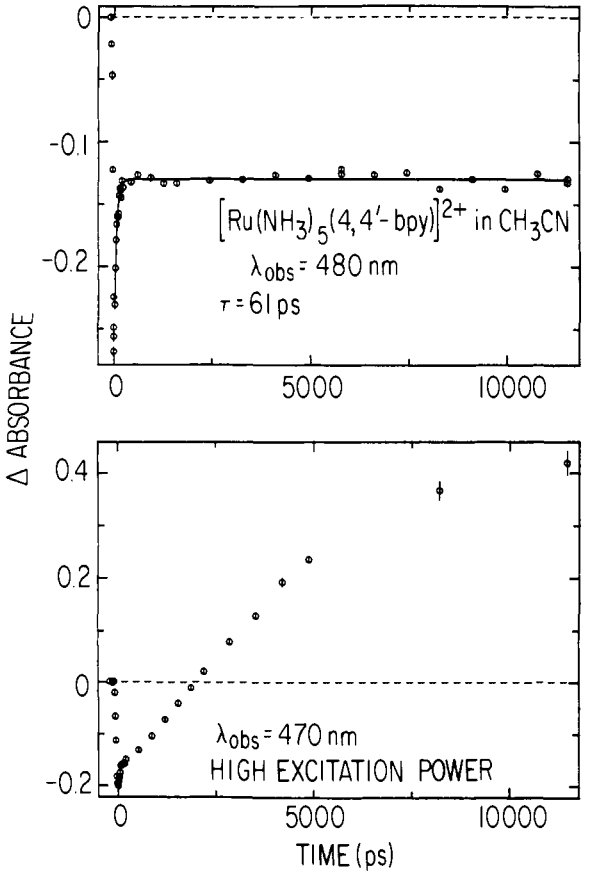

Figure 5. Transient kinetics for $[Ru(NH_3)_5(4,4'\text{-bpy})]X_2$ in CH_3CN. Upper: [Ru(II)] = 5×10^{-4} M, X = $CF_3SO_3^-$, observation wavelength (λ_{obs}) = 480 ns, low-power excitation conditions; solid curve is a single exponential decay function with a rate constant $k = 1.6 \times 10^{10}$ s^{-1}. Lower: [Ru(II)] = 2×10^{-4} M, X = PF_6^-, λ_{obs} = 470 nm, high-power excitation conditions.

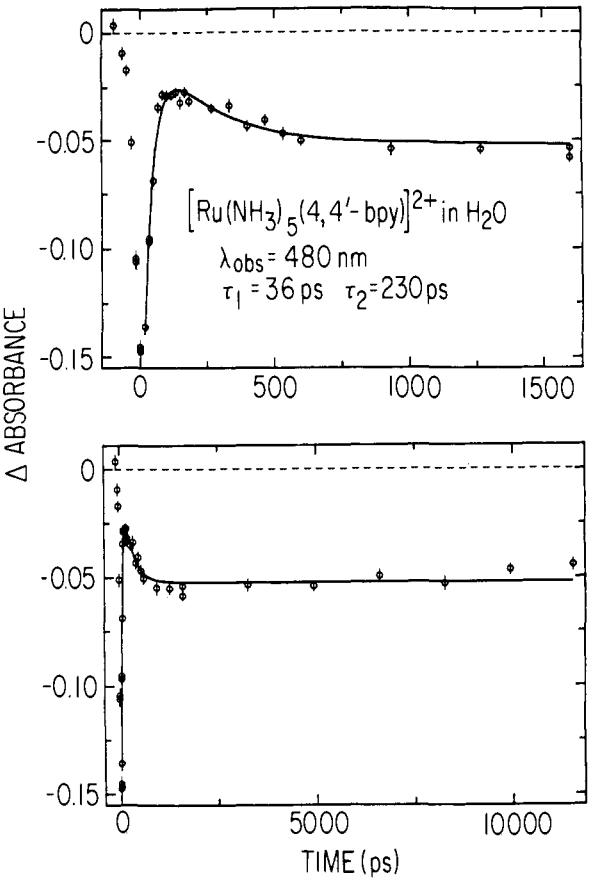

Figure 6. Transient kinetics for $[Ru(NH_3)_5(4,4'\text{-bpy})](CF_3SO_3)_2$ in H_2O (5×10^{-4} M), recorded at 480 nm. Solid curve is a double exponential decay function with rate constants $k_1 = 2.8 \times 10^{10}$ s^{-1} and $k_2 = 4.3 \times 10^9$ s^{-1}. The upper and lower plots differ only in the abscissa scales.

Pentaammineruthenium(II) Complexes. The quantum yields for NH_3 loss from $Ru^{II}(NH_3)_5L$ with L = 4,4'-bpy at pH 7 are $(7 \pm 5) \times 10^{-3}$ with λ_{exc} = 500 nm and 0.22 for λ_{exc} = 254 nm. For L = 4,4'-bpyH$^+$ at pH 1, ϕ_{NH_3} is $(4 \pm 3) \times 10^{-3}$ with λ_{exc} = 560 nm. Reduction potentials, taken as the average of cathodic and anodic peak positions in cyclic voltammograms, are summarized in Table I. Where comparison is possible, these data are in good agreement with those reported in other work.[5] Vis-NIR spectra for $Ru(NH_3)_5(pzCH_3)^{3+}$ in water (D_2O) and Me_2SO are presented in Figure 4. The NIR band for $Ru(NH_3)_5(pzH)^{3+}$ in 0.1 M DCl is virtually superposable on that for the $pzCH_3^+$ complex, in agreement with the results of Magnuson and Taube.[15]

In ns flash-photolysis experiments[11,12] (λ_{exc} = 532 nm, pulse width (fwhm) = 20 ns) small yields of transients with spectra identical with those of the protonated species $(NH_3)_5RuLH^{3+}$ were detected after excitation of $(NH_3)_5RuL^{2+}$. For L = pz with $I_{in} \sim 10^2$ einsteins cm^{-2} s^{-1}, the yield of protonated complex was 0.02–0.05 based on initial ground-state concentration. In the pH range 3–7 the transient $(NH_3)_5Ru(pzH)^{3+}$ decayed with a rate constant of $(2\text{–}3) \times 10^7$ s^{-1}. With L = 4,4'-bpy the $(NH_3)_5Ru(4,4'\text{-bpyH})^{3+}$ decay rate constant was $\sim 2 \times 10^5$ s^{-1} (pH 7–10, dilute buffers).

Mulitphoton Artifacts in the ps Photolysis of Pentaammineruthenium(II) Complexes. Figure 5 presents kinetics results for $Ru(NH_3)_5(4,4'\text{-bpy})^{2+}$ in acetonitrile at 480 (top) and 470 (bottom) nm. The 480-nm data were acquired with ~0.8 mJ of excitation energy per 532-nm pulse, while the 470-nm data were obtained at higher power. The absorbance increase after 2.5 ns is characteristic of multiphoton excitation in this and related complexes. By contrast, at very low powers a bleach is observed at 470 nm. The ratio of the t = 11.5 ns and 0 signals at 470 nm increases strongly with excitation intensity (supplementary Figure

(15) Magnuson, R. H.; Taube, H. *J. Am. Chem. Soc.* **1975**, *97*, 5129.

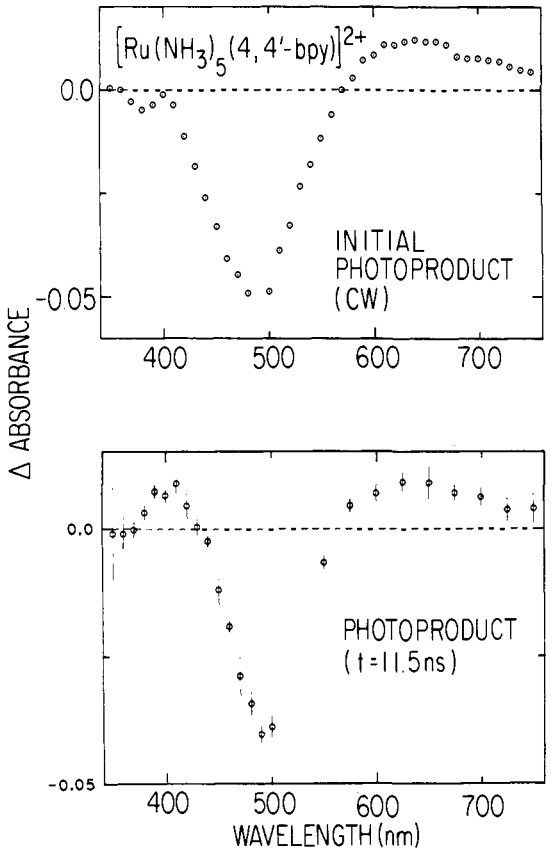

Figure 7. Difference spectra of $[Ru(NH_3)_5(4,4'\text{-bpy})]^{2+}$ in water. Upper: After CW photoexcitation at $\lambda > 500$ nm, [Ru(II)] = 7×10^{-4} M, cell path length = 0.2 cm. Lower: recorded 11.5 ns after 532-nm laser excitation, [Ru(II)] = 4×10^{-4} M, cell path length = 0.2 cm.

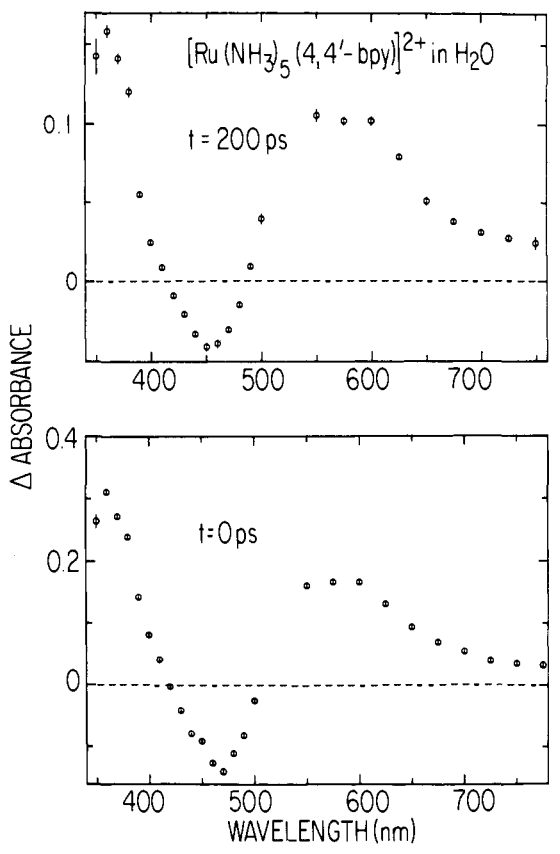

Figure 8. Transient ground-state difference spectra for $Ru(NH_3)_5(4,4'\text{-bpy})^{2+}$ at 200 and 33 ps in water solvent.

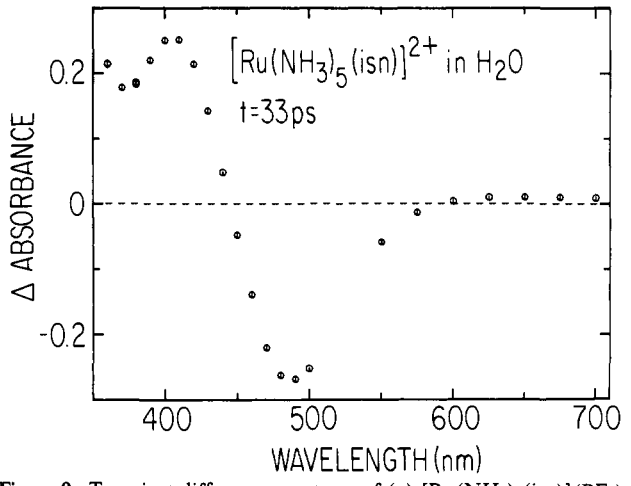

Figure 9. Transient difference spectrum of (a) $[Ru(NH_3)_5(isn)](PF_6)_2$ in H_2O (4×10^{-4} M), recorded 33 ps after 532-nm laser excitation.

1) which would not be true if both signals arose from a one-photon excitation process.

$Ru(NH_3)_5(4,4'\text{-bpy})^{2+}$. Figure 6 presents "low-power" (~0.8 mJ per 532-nm pulse) excitation kinetics results for $Ru(NH_3)_5(4,4'\text{-bpy})^{2+}$ in water.[16] The initial 61-ps decay in Figure 5 (top) for this complex in acetonitrile is replaced in water by two decays: a pulse-width-limited decay of $\lesssim$36 ps and a longer decay of 230 ps. In both solvents permanent (>10 ns) loss of ground state is observed.

Several observations show that the >10-ns ground-state loss is due to formation of "permanent" products—in water $Ru(NH_3)_4(OH_2)(4,4'\text{-bpy})^{2+}$ (cis or trans) and, possibly, smaller amounts of $Ru(NH_3)_5OH_2^{2+}$. That relatively high NH_3 yields are produced under ps excitation was established as follows: an aqueous solution of $Ru(NH_3)_5(4,4'\text{-bpy})^{2+}$ (50 mL) was repetitively excited under standard conditions so that effectively 60% of the solution (excitation volume × number of shots) was exposed to ps-laser pulses. The yield of NH_3 released was 0.04 (2), based on the initial concentration of the complex. The laser power was adjusted such that about half the molecules in the excitation volume ($\sim 4 \times 10^{-3}$ mL) were excited during a pulse. Thus an apparent one-photon quantum yield of 0.13 (6) (about 20 times greater than under continuous photolysis conditions) is obtained. In addition, both the >10-ns spectrum from ps excitation and the initial photoproduct difference spectrum from the Xe-lamp continuous-photolysis experiment (Figure 7) are consistent with NH_3 loss to give $Ru(NH_3)_4(OH_2)L^{2+}$: while L loss would lead to uniform bleaching of ground-state absorption ($Ru(NH_3)_5OH_2^{2+}$ does not absorb in the visible), NH_3 loss should lead only to slight spectral shifts with increased absorption in some spectral regions and bleaching in others—as is seen in Figure 7. Indeed if the NH_3 yield is used as an estimate of $Ru(NH_3)_5L^{2+}$ loss, the absorbance data in Figure 7, corrected for $Ru(NH_3)_5L^{2+}$ loss, give a photoproduct spectrum very similar to that of the starting complex, as is expected for $Ru(NH_3)_4(OH_2)L^{2+}$ as the major product. As discussed later, this high yield of photoproduct (~0.1) is ascribed to multiphoton processes which evidently persist even in this "low-power" region. Picosecond photolysis with L = 4,4'-bpyH$^+$ also led to high apparent photolysis yields at "low-power", but negligible photoaquation was found for the other complexes studied (except pyridine, vide infra).

Transient spectral data for $Ru(NH_3)_5(4,4'\text{-bpy})^{2+}$ in water at ~0 and 200 ps are shown in Figure 8. Supplementary Figures 2–4 present "low-power" excitation kinetics results for $Ru^{II}(NH_3)_5L$; for L = pzH$^+$, 4,4'-bpyH$^+$, and 4-acpy in water, the ex-

(16) The $Ru(NH_3)_5(4,4'\text{-bpy})^{2+}$ sample absorbed ~60% of the incident photons yielding a maximum number of excited molecules of $\sim 2.1 \times 10^{-9}$ mol per pulse. There were $\sim 2.0 \times 10^{-9}$ mol of sample in the path of each pulse. Therefore the *maximum* fraction of ground-state molecules excited is ~100%. Since the ϵ at 532 nm for $Ru(NH_3)_5(4,4'\text{-bpy})^{2+}$ is ~2 times as large as that of $Ru(tpy)_2^{2+}$, a somewhat higher (i.e., 80% vs. 60%) fractional excitation of the $Ru(NH_3)_5(4,4'\text{-bpy})^{2+}$ sample is very likely.

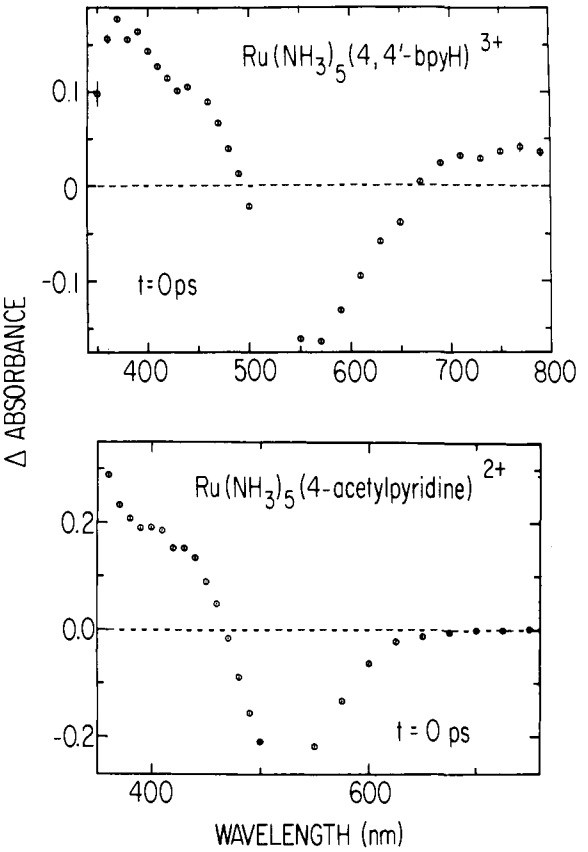

Figure 10. Transient difference spectra of 4,4'-bpyH$^+$ (2×10^{-4} M in 0.1 M HCl) (top) and 4-acetylpyridine (3×10^{-4} M) complexes recorded during the ~30-ps 532-nm pulse.

Table II. Summary of Lifetimes of Transients Produced in ps Experiments[a]

complex	$10^{-3}\epsilon_{exc}$, M^{-1} cm^{-1}	τ, ps	assignment
$Ru(tpy)_2^{2+}$	3	250	MLCT
$Ru(NH_3)_5L^{2+}$			
py	3	$\ll 20^b$	MLCT
4-C_6H_5py	1	~450	MLCT
isn	4	140	
pz	4	225	MLCT
4,4'-bpy	6	<36, 230[b]	MLCT
		60[b,c]	MLCT
4,4'-bpyH$^+$	11	<30[b]	MLCT
pzH$^+$	15	<30	MLCT
pzCH$_3^+$	15	<30	MLCT

[a] For room-temperature aqueous solutions; λ_{exc} = 532 nm except for $Ru(NH_3)_5py^{2+}$ (λ_{exc} = 355 nm). ϵ_{exc} is the molar absorptivity of the ground state at λ_{exc}. [b] Permanent photoproduct (e.g., photoaquation) also observed. [c] In acetonitrile solvent.

cited-state lifetime is $\tau \leq 30$ ps (pulse-width limited). For L = pz and isn the excited-state lifetimes are 225 and 140 ps, respectively. With 532-nm excitation of the 4-phenylpyridine complex a relatively long-lived transient (τ ~440 ps) was observed; its spectrum resembled the 4,4'-bpy transient spectrum. For L = py, small-amplitude bleaching of the ground-state absorbance was observed during the 355-nm excitation pulse and permanent $Ru(NH_3)_5py^{2+}$ loss was evident at the end of the pulse (supplementary Figure 5). Figures 9–11 present initial transient difference spectra for L = isn, 4-acpy, 4,4'-bpyH$^+$, pz, and pzH$^+$.

The lifetimes of the transients observed in the ps experiments are summarized in Table II; their assignments are discussed next.

Discussion

Transient Assignments. Studies of $M(bpy)_3^{2+}$ complexes (M = Ru, Os; bpy = 2,2'-bipyridine) have shown that the spectra of their MLCT excited states can be modeled in terms of the $M^{III}L^{\bullet-}$ chromophore[12,17] with $L^{\bullet-}$ intraligand transitions providing a distinctive signature. The $Ru(tpy)_2^{2+}$ transient spectrum (Figure 3) strongly resembles[12,17] that of $*Ru(bpy)_3^{2+}$ (the MLCT state of $Ru(bpy)_3^{2+}$) especially in the intense ~390-nm band. Thus the expected MLCT character of the 250-ps excited state of $Ru(tpy)_2^{2+}$ is supported by the ps spectral data.

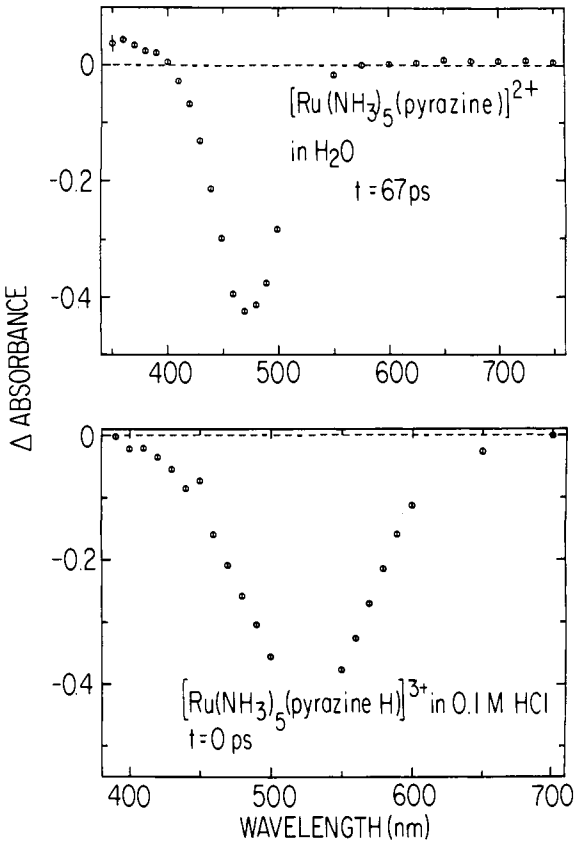

Figure 11. Transient difference spectra of pyrazine (top) and protonated pyrazine complexes recorded at 67 and 0 ps, respectively.

Extending the above analogy to the pentaammine complexes, the $Ru(NH_3)_5L^{2+}$ MLCT state is modeled as $Ru^{III}(NH_3)_5(L^{\bullet-})^{2+}$ and the MLCT state should have absorptions due to the ($L^{\bullet-}$) chromophore. Models for the $L^{\bullet-}$ spectra are taken from the pulse-radiolysis literature.[18] The spectrum of the protonated pyrazine radical pzH$^\bullet$ has a band at ~290 nm ($\epsilon \approx 5000$ M^{-1} cm^{-1}) but no appreciable absorption for $\lambda > 350$ nm.[18] As expected for an $(L^{\bullet-})H^+$ model of the MLCT states of $Ru(NH_3)_5pz^{2+}$ and $Ru(NH_3)_5(pzH)^{3+}$, the first transients observed exhibit only ground-state bleaching in the 350–700-nm region (Figure 11). By contrast, protonated isonicotinamide radical (isnH$^\bullet$) has strong absorption bands at 300 nm ($\epsilon \approx 10\,000$ M^{-1} cm^{-1}) and at 400 nm ($\epsilon \approx 7000$ M^{-1} cm^{-1}).[18] Thus the MLCT state of $Ru(NH_3)_5isn^{2+}$ should show moderately intense absorption in the 400-nm region. As is evident in Figure 9, the transient spectrum observed for $Ru(NH_3)_5isn^{2+}$ shows both ground-state bleaching at 490 nm and increased absorptions at 400 nm. Also, the absorbance increase is ~90% as large as the magnitude of the bleach at 490 nm, consistent with a $Ru^{III}(NH_3)_5(isn^{\bullet-})^{2+}$ formulation of the excited state.

The spectrum of 4,4'-bpyH$^\bullet$ in water[18] is shown in Figure 12. This radical has a moderately intense absorption band at 570 nm and a narrow, intense band at 380 nm. In Figure 8 both transient spectra for $Ru(NH_3)_5(4,4'\text{-bpy})^{2+}$ in water show a large absorbance increase at 580 nm, a slightly smaller bleach at 470 nm, and a very intense 360-nm band. These are exactly the features

(17) Sutin, N.; Creutz, C. *Adv. Chem. Ser.* **1978**, *168*, 1.
(18) Moorthy, P. N.; Hayon, E. *J. Phys. Chem.* **1974**, *78*, 2615 (L = pz). Cercek, B.; Ebert, M. *Trans. Faraday Soc.* **1967**, *63*, 1687 (L = py). Simic, M.; Ebert, M. *Int. J. Radiat. Phys. Chem.* **1971**, *3*, 259 (L = 4,4'-bpy, isn, and others).

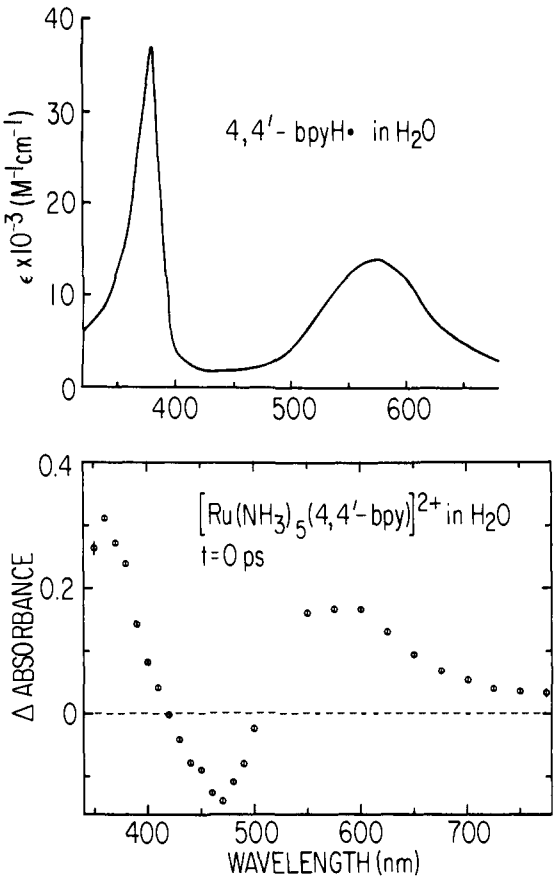

Figure 12. Absorption spectrum of protonated 4,4′-bipyridine radical generated by pulse radiolysis in aqueous solution adapted from ref 18 (top) and transient difference spectrum of $[Ru(NH_3)_5(4,4'\text{-bpy})](CF_3SO_3)_2$ in H_2O (4×10^{-4} M) recorded during 532-nm laser excitation.

expected for an MLCT state of this complex. Thus the spectral comparisons provide strong evidence for assigning the first transients produced with 532-nm excitation as MLCT states. For $Ru(NH_3)_5py^{2+}$ (λ_{max} = 407 nm, 355-nm excitation) the first transient was barely detectable. Since the MLCT state of this complex should not absorb at $\lambda > 400$ nm, the small amplitude of the bleaching at 410 nm during photoexcitation (supplementary Figure 5) suggests a very short lifetime ($\tau \ll 20$ ps) for the MLCT state of this complex.

As noted earlier, two transients ($\tau \leq 36$ and 230 ps) are found for $Ru(NH_3)_5(4,4'\text{-bpy})^{2+}$. The spectra obtained during the ~25-ps pulse and at 200 ps are qualitatively very similar but differ in amplitude (Figure 8). In particular, the ratio of transient absorbance increases at 390 or 600 nm to the bleach at ~450 nm is much greater in the later spectrum. A number of relaxation processes might be considered for the ≤36-ps process—for example, solvent relaxation of the Franck–Condon MLCT state or intersystem crossing of the initially formed singlet to the triplet state. An interesting alternative involving a "conformation change" of the ligand might also be considered in light of the fact that the rapid relaxation is found only for the 4,4′-bpy complex. In ground-state $Ru(NH_3)_5(4,4'\text{-bpy})^{2+}$ the two pyridine rings may be canted with respect to each other.[19] However, in the 4,4′-bpy radical anion coplanarity of the rings is more strongly favored because of the increased bond order of the interring C–C bond.[20] The rapid relaxation ($>10^{11}$ s^{-1}) could then correspond to a twist toward the coplanar configuration, with the process spectrally detectable because vis-near-UV electronic transitions of the planar radical are more intense than in the (less conjugated) twisted form. By contrast, in acetonitrile such relaxation is not directly observed and the lowest energy MLCT state lives only 60 ps. Nor is biphasic behavior found for the structurally related 4-phenylpyridine complex in water.

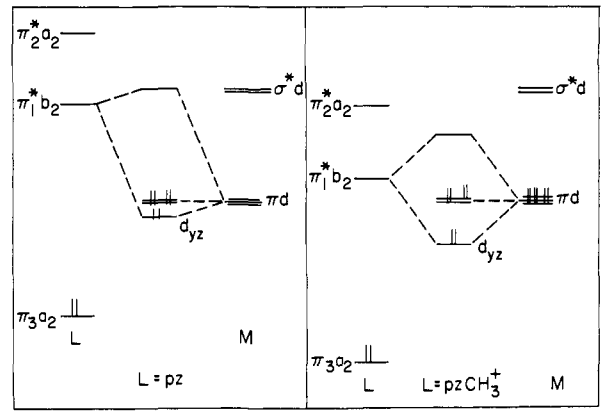

Figure 13. Orbital diagrams for $Ru(NH_3)_5pz^{2+}$ and $Ru(NH_3)_5(pzCH_3)^{3+}$.

Except for L = 4,4′-bpy in water (see above) all transient decays observed in this study were monophasic within experimental error. In light of Ford's photochemical results,[6] LF population should result from initial MLCT excitation of the complexes with shorter wavelength MLCT maxima, i.e., L = py and 4-phenylpyridine in the present study. In neither case was a transient ascribable to the LF state detected, suggesting $\tau(LF) \ll 20$ ps and $\tau(LF) < 450$ ps ($\tau(LF) < \tau(MLCT)$) for py and 4-phenylpyridine, respectively, provided that the spectra of the LF states differ significantly (on the order of 20%, depending on the complex) from those of the aquated photoproducts or the $Ru(NH_3)_5L^{2+}$ ground states. (In addition the susceptibility of these complexes to multiphoton excitation makes the reliable interpretation of long-time signals difficult, e.g. Figure 5.)

Properties of the $Ru(NH_3)_5L^{2+}$ Ground and Excited States. The ground-state spectra of $Ru(NH_3)_5L^{2+}$ compelxes are dominated by intense ($\epsilon \geq 10^4$ M^{-1} cm^{-1}) visible bands which are sensitive to both the solvent and the substituents on L. Both solvent and substituent sensitivity may be understood in terms of the metal-to-ligand charge-transfer assignment: substituents alter[4] the electron-acceptor ability ($E°_{L/L^-}$) of the ligand as shown in Table I. Band shifts with solvent arise largely[5] because the electron-donor ability ($E°_{Ru^{III}L/Ru^{II}L}$) of the pentaammineruthenium moiety is very solvent dependent while the acceptor ability of L is not.[5]

Orbital diagrams[10,15,21] for Ru^{II}–pz and Ru^{II}–$pzCH_3^+$ combinations are given in figure 13 in which the M–L bond is taken as the z axis (C_{2v} symmetry). (The diagrams for L = isn, 4,4′-bpy, and 4-acpy are similar to that for L = pz.) For L = pz and $pzCH_3^+$, the two lower π^* orbitals b_2 and a_2 are split by ca. 10000 cm^{-1},[22] with b_2 being lower. Furthermore, since a_2 has nodes on the nitrogen atoms while b_2 does not, Ru(II) πd–pz $b_2\pi^*$ interaction is expected to be the greater. This interaction results in the splitting of the πd orbitals with d_{yz} (b_2) lying lower. For L = pz, isn, etc., the ground-state HOMO is viewed as largely metal centered.[21,23] With L = $pzCH_3^+$ or pzH^+, the interactions are

(19) Spotswood, T. McL.; Tanzer, C. I. *Aust. J. Chem.* **1967**, *20*, 1227. Cf.: Akiyama, M.; Watanabe, T.; Kakihana, M. *J. Phys. Chem.* **1986**, *90*, 1752 (an evaluation of the barrier to internal rotation in biphenyl); Schanze, K. S.; Neyhart, G. A.; Meyer, T. J. *J. Phys. Chem.* **1983**, *90*, 2182 (in which 4,4′-bpy internal rotation is implicated in binuclear complexes related to this system).

(20) Lee, P. C.; Schmidt, K.; Gordon, S.; Meisel, D. *Chem. Phys. Lett.* **1981**, *80*, 242.

(21) Zwickel, A. M.; Creutz, C. *Inorg. Chem.* **1971**, *10*, 2395.

(22) The first two π,π^* transitions in pz lie at 38800 and 51000 cm^{-1}: Parkin, J. E.; Innes, K. K. *J. Mol. Spectrosc.* **1965**, *15*, 407.

(23) These conclusions are also supported by the band intensities. The MLCT band oscillator strengths f are evaluated from $f = (4.6 \times 10^{-9})\epsilon\Delta\bar{\nu}_{1/2}$ where ϵ is the molar absorptivity and $\Delta\bar{\nu}_{1/2}$ is the width (in cm^{-1}) at half intensity: [L, $\epsilon(M^{-1}\,cm^{-1})$, $\Delta\bar{\nu}_{1/2}$ (cm^{-1}), f] py, 7.8×10^3, 4.3×10^3, 0.154; isn, 1.05×10^4, 4.0×10^3, 0.193; pz, 1.37×10^4, 3.2×10^3, 0.233 (in water). Then, in a one-electron model, the M–L orbital mixing coefficient α may be evaluated from $f = (1.09 \times 10^{-5})\bar{\nu}_{max}\, r^2\alpha^2$ where $\bar{\nu}_{max}$ is the position of the MLCT band in cm^{-1} and r is the charge-transfer distance in Å. The α^2 values 0.047 (py), 0.069 (isn), and 0.072 (pz) obtained assuming r = 3.5 Å are in excellent agreement with those given in ref 21.

qualitatively the same, but recent structural results,[24] the electrochemical data in Table I, and the spectral data indicate much stronger π-back-bonding (greater Ru–L mixing) as is indicated in Figure 13.

For L = pz, py, isn, etc., *one* MLCT transition is observed.[4,21,15] Charge-transfer transitions from any of the πd set to Lπ^* b_2 and a_2 orbitals are allowed except $\pi d_{xz} \rightarrow b_2\pi^*$, but the most intense is expected to be $d_{yz} \rightarrow L\pi^*(b_2)$ because the spatial overlap between donor and acceptor orbitals is greatest for this transition.[25] By contrast, with L = $pzCH_3^+$ or pzH^+ an additional weak (oscillator strength 0.029) band (ν_2) is observed[15] at much lower energy as is shown in Figure 4. An MLCT assignment for this band is suggested by its shape ($\Delta\bar{\nu}_{1/2}$ = 3900 cm^{-1}), which resembles that of the $Ru(NH_3)_5L^{2+}$ visible bands (typical $\Delta\bar{\nu}_{1/2}$ = 3200–4600 cm^{-1}),[4,10,23] and by its solvent sensitivity. As is generally found[4,5] for $Ru(NH_3)_5L^{2+}$, the band shifts to longer wavelength (lower energy) on going from water (D_2O) to dimethyl sulfoxide. Remarkably, for L = $pzCH_3^+$ the position of the (538 nm) visible band (oscillator strength 0.28) is the same in the two solvents. These observations are consistent with the ground-state orbital diagram in Figure 13 and with the interpretation given earlier by Magnuson and Taube.[15] Within this model, the visible band arises through excitation from a π-bonding d_{yz} orbital and, the NIR transition, through excitation from a non-π-bonding d_{xy} orbital. For L = $pzCH_3^+$ the zero-order energy difference between πd and ligand $b_2\pi^*$ orbitals is small, the ensuing mixing greater, and the resulting πd splitting greater than for L = pz, etc. Indeed, π-interaction is so great that the principal absorption band is essentially a bonding-to-antibonding ("π,π^*") transition between extensively delocalized molecular orbitals. As a consequence, the charge-transfer character of this transition is greatly reduced and this is reflected in the solvent insensitivity of the band. By contrast, the lower energy band (which may be thought of as a "n $\rightarrow$ (M–L)π^*" transition) retains solvent sensitivity because charge transfer *does* result when the transition is from a nonbonding d_{xy} (rather than d_{yz}) orbital. The energy difference between the two transitions, $\bar{\nu}_1 - \bar{\nu}_2 \geq 7000$ cm^{-1} (depending upon solvent), reflects the excited-state splitting between d_{yz} and d_{xy} at ground-state nuclear configuration and is large indeed. Thus metal–ligand "double bonding" (Ru=N) is strongly suggested.

Recently, trends in (singlet) MLCT absorption band maxima and ground-state redox potentials ($\Delta E = E_{M^+/M} = E_{L/L^-}$) have been exploited in assigning spectra and modeling excited-state lifetimes.[26,27] For the present series of complexes it is worth noting reasonable agreement with this trend for L = pz and $pzCH_3^+$. From the data in Table I ΔE(pz) = 2.57 V (with E_{L/L^-} approximated by the redox potential of the free ligand) and $\Delta E(pzCH_3^+)$ = 1.64 V; from the MLCT band maxima the values 2.64 eV (pz) and 1.41 eV ($pzCH_3^+$; ν_2 in water) are obtained.

Excited-State Protonation. Ford et al.[4] estimated the pK_a of the $Ru(NH_3)_5pzH^{3+}$ MLCT excited state from the ground-state pK_a (2.6) and the separation in visible band maxima found for L = pz and pzH^+. Their estimated value (7.4) refers to the higher excited state originating from π-bonding d (d_{xy})-to-Lπ^* excitation. For completeness we also consider the acidity of the lower pzH^+ excited state (ν_2): with ν_2 = 11.4 × 10^3 cm^{-1} for pzH^+ and ν = 21.2 × 10^3 cm^{-1} for pz[4] (in water) the acid/base Franck–Condon CT excited-state energy difference is then 9.8 × 10^3 cm^{-1} (1.21 eV or 20.6 pK_a units) which yields a pK_a estimate of 23.2 for the $Ru(NH_3)_5pzH^{3+}$ excited state arising from "nonbonding"-d-to-L(π^*) excitation. The first and second pK_a values of pzH_2^+ (diprotonated pyrazine radical anion) are 10.5 and >15, respectively.[18] The four values reflect qualitatively the increased electron density on the $pzH^\bullet$ moiety compared to that of pz for which pK_a values are −5.8 and 0.7.[28] Spectroscopic information has also been used to estimate that the pK_a for the MLCT state of $Ru(NH_3)_5(4,4'\text{-bpyH})^{3+}$ is 11.6; the ground-state pK_a is 4.7.[10]

As noted earlier with L = pz and 4,4′-bpy, small yields of the protonated species $Ru(NH_3)_5LH^{3+}$ were detected after excitation of $Ru(NH_3)_5L^{2+}$ (in water) with 20-ns, 530-nm light pulses. This assignment of the transients in the flash-photolysis experiments is based on their absorption spectra and is supported by the transient decay rates.[29] The latter are ascribed to eq 1. With

$$Ru(NH_3)_5LH^{3+} + H_2O \underset{}{\overset{k_1}{\rightleftharpoons}} Ru(NH_3)_5L^{2+} + H_3O^+ \quad (1)$$

L = pz, the transient decayed with a rate constant (2.5 ± 0.5) × 10^7 s^{-1} in the pH range 3–7. This rate constant is a reasonable one for k_1 (L = pz) given that[4] K_1 = 3 × 10^{-3} M and assuming $k_{-1} \geq 1 \times 10^{10}$ M^{-1} s^{-1}. With L = 4,4′-bpy ($K_1 = 2 \times 10^{-5}$ M)[10] the $(NH_3)_5Ru(4,4'\text{-bpyH})^{3+}$ decay rate constant of ~2 × 10^5 s^{-1} (pH 7–10 dilute buffers) is also consistent with that expected for k_1, again assuming k_{-1} to be ≥1 × 10^{10} M^{-1} s^{-1}. Although the involvement of multiphoton processes cannot be ruled out in these experiments, the small yields of $Ru(NH_3)_5LH^{3+}$ are reasonably ascribed to MLCT excited-state protonation: eq 2–4, protonation of the ~200-ps MLCT excited state of $Ru(NH_3)_5L^{2+}$ ($^*Ru(NH_3)_5L^{2+}$) by water, followed by rapid deactivation of the protonated excited state, provides a mechanism for $Ru(NH_3)_5LH^{3+}$ formation. Because proton loss from Ru-

$$h\nu + Ru(NH_3)_5L^{2+} \xrightarrow{k_1} {}^*Ru(NH_3)_5L^{2+} \quad (2)$$

$$^*Ru(NH_3)_5L^{2+} + H_2O \xrightarrow{k_3} {}^*Ru(NH_3)_5LH^{3+} + OH^- \quad (3)$$

$$^*Ru(NH_3)_5L^{2+} \xrightarrow{1/\tau_4} Ru(NH_3)_5L^{2+} \qquad \tau_4 \sim 200 \text{ ps} \quad (4)$$

$$^*Ru(NH_3)_5LH^{3+} \xrightarrow{1/\tau_5} Ru(NH_3)_5LH^{3+} \qquad \tau_5 < 30 \text{ ps} \quad (5)$$

$(NH_3)_5LH^{3+}$ (eq 1) is "slow" and the decays of the pentaammine MLCT states are rapid, many opportunities for (re-)excitation of $Ru(NH_3)_5L^{2+}$ and eq 3 and 5 occur during the 20-ns excitation. (By contrast, in the ps experiment there is only one opportunity for population of $^*Ru(NH_3)_5L^{2+}$ and protonation via eq 3.) Provided that $1/\tau_5 \gg k_3, k_1$, the yield of protonated species within this model is given by eq 6,[12] where Δt is the length of the laser

$$Y_H = (k_1\Delta t)k_3/(k_3 + 1/\tau_4) \quad (6)$$

pulse (20 ns) and k_1 is the excitation rate constant (a function of light intensity and the ground-state molar absorptivity at the exciting wavelength;[12] typically ~10^9 s^{-1} for L = pz in the present experiments). For $Ru(NH_3)_5pz^{2+}$, the yield of protonated complex Y_H = 0.02–0.05, with $1/\tau_4 = 5 \times 10^9$ s^{-1}, gives $k_3 \sim 1 \times 10^7$ s^{-1}. With such a relatively low k_3 value, only very small yields of $Ru(NH_3)_5pzH^{3+}$, $k_3\tau_4 \sim 2 \times 10^{-3}$, should be produced on ps excitation and the fact that none is detected is consistent with this protonation rate constant. Provided that eq 2–5 provide a correct model for $Ru(NH_3)_5pzH^{3+}$ formation, these observations can be used to estimate an effective excited-state pK_a. If k_{-3} is assumed to be diffusion-controlled ($k_{-3} \sim 5 \times 10^{10}$ M^{-1} s^{-1}), then K_3 = 2 × 10^{-4} M, and the equilibrium constant for eq 7 is 2 × 10^{10} M^{-1}

$$^*Ru(NH_3)_5pz^{2+} + H_3O^+ \rightleftharpoons {}^*Ru(NH_3)_5pzH^{3+} + H_2O \quad (7)$$

so that the apparent pK_a of $^*Ru(NH_3)_5pzH^{3+}$ is 10.3. This pK_a value is close to that obtained above for the Franck–Condon state of the higher (ν_1) L = pzH^+ excited state (pK_a = 7.4) and is also about the same as pK_{a1} for $pzH_2^{\bullet+}$. (The inferred value for k_3 ~ 1 × 10^7 s^{-1} is also essentially identical with the rate constant,

(24) Wishart, J.; Bino, A.; Taube, H. *Inorg. Chem.* **1986**, *25*, 3318.

(25) (a) Provided that the "ruthenium(III)" in the MLCT excited state has the $(d_{xz})^2(d_{xy})^2(d_{yz})^1$ configuration,[25b] the most intense MLCT transition will also be the lowest energy transition. Thus transitions arising from excitation of the non-π-bonding d_{xz} and d_{xy} electrons would occur to higher energy. While the visible MLCT bands for these complexes are asymmetric with higher intensity on the the high energy side, this broadening could arise from other sources.[4] (b) EPR studies of $Ru(NH_3)_5pz^{3+}$ are consistent with this lowest energy configuration. See: Dubicki, L.; Ferguson, J.; Krausz, E. R. *J. Am. Chem. Soc.* **1985**, *107*, 179.

(26) Johnson, C. R.; Shepherd, R. E. *Inorg. Chem.* **1983**, *22*, 2439. Caspar, J. V.; Meyer, T. J. *Inorg. Chem.* **1983**, *22*, 2444.

(27) Creutz, C. *Comments Inorg. Chem.* **1982**, *1*, 293. Dodsworth, E. S.; Lever, A. B. P. *Chem. Phys. Lett.* **1986**, *124*, 152 and references cited therein.

(28) Cha, A. S.-C.; Trimble, R. F., Jr. *J. Phys. Chem.* **1961**, *65*, 863.

(29) For L = 4,4′-bpy this interpretation is also supported by resonance raman studies: Caswell, D. S.; Spiro, T. G. *Inorg. Chem.* **1987**, *26*, 18.

Table III. Ligand-Field Parameters for Low-Spin d^6 Complexes in Units of 10^3 cm^{-1}

complex	Δ_0	B	C	C/B	$\Delta_{ST}(T_1)$	$E^*(^3T_1)$	$\lambda^*(^3T_1)$	ref
$Ru(H_2O)_6^{2+}$	21.8	0.500	2.8	5.6	5.6			*a*
$Co(NH_3)_6^{3+}$	24.0	0.619	3.7	5.9	7.3	10.1	2.8	*b*
$Nb(CO)_6^-$	25.2		0.8		1.6	19.9	2.8	*c*
$Co(CN)_6^{3-}$	34.8	0.400	2.7	6.8	5.4	20.7	6.0	*d*
$Rh(en)_3^{3+}$	36.4	0.356	2.6	7.3	5.2	22.8	5.8	*e*
$Ir(en)_3^{3+}$	43.7	0.318	2.9	9.1	5.8	25.4	8.6	*e*
$Ru(NH_3)_6^{2+}$	(28.3)	0.414	(2.7)	(6.5)	(5.4)	(16.6)	(3.6)	*f*

[a] Bernhard, P. Ph.D. Thesis, University of Bern, 1984. [b] Wilson, R. B.; Solomon, E. I. *J. Am. Chem. Soc.* **1980**, *102*, 4085. [c] Beach, N. A.; Gray, H. B. *J. Am. Chem. Soc.* **1968**, *90*, 5713. Geoffroy, G. L.; Wrighton, M. S. *Organometallic Photochemistry*; Academic Press: New York, 1979, Chapter 2. [d] Miskowski, V. M.; Gray, H. B.; Wilson, R. B.; Solomon, E. I. *Inorg. Chem.* **1979**, *18*, 1410. [e] DeArmond, M. K.; Hillis, J. E. *J. Chem. Phys.* **1971**, *54*, 2247. [f] Values in parentheses are calculated from the positions of the observed spin-allowed transitions (290 and 310 nm, ref 37) with the assumption $C = 2700$ cm^{-1} and neglect of the terms in B^2/Δ_0. The λ^* estimate (used to obtain E^*) was obtained from $\lambda^* = 4.5 \times 10^{-6}(\Delta_0)^2$, a relationship which is found for the five entries above $Ru(NH_3)_6^{2+}$ in this table.

7×10^6 s^{-1}, for protonation of $pzH^{\bullet}$ by water to yield $pzH_2^{\bullet+}$.[27]) The three-unit pK_a discrepancy between the value estimated from the kinetics and that estimated from the spectra for the Franck–Condon excited states could be due to equilibrated-MLCT-excited-state energy differences ($\sim 1.4 \times 10^3$ cm^{-1}) not reflected in the absorption maxima as well as to errors in the "kinetic" pK_a value.

MLCT Excited-State Energies. The visible (NIR) band maxima of the $Ru(NH_3)_5L^{2+}$ complexes reflect the positions E_{op} of Franck–Condon MLCT (or, for L = $pzCH_3^+$ or pzH^+, $\pi,\pi^*/n,\pi^*$) states produced directly from light absorption. As these have the same nuclear configurations as ground-state $Ru(NH_3)_5L^{2+}$, the thermally equilibrated excited (thexi) states in which solvent and metal–ligand and intraligand positions have relaxed lie at lower energy E^*. Defining λ^* as the distortion energy of the Franck–Condon excited state, $E_{op} = E^* + \lambda^*$. For $Ru(bpy)_3^{2+}$ and related complexes detailed analyses of (structured) emission spectra suggest $\lambda^* \sim 2400$ cm^{-1} in fluid solution at room temperature.[30] λ^* is comprised of intraligand (λ_{IL}^*), metal–ligand (λ_{ML}^*), and outer-shell (solvent) λ_o^* contributions (~ 1350, ~ 500, and ~ 500 cm^{-1}, respectively,[30a] for $Ru(bpy)_3^{2+}$). For $Ru(NH_3)_5L^{2+}$ the lack of structured absorption and emission spectra makes "direct" experimental evaluation of these distortion parameters extremely difficult. However, consideration of related systems and analyses of the absorption band shapes enable estimates to be made as follows: From studies of Ru(II) and Os(II) polypyridine complexes[30] $\lambda_{IL}^* = 500$–1500 cm^{-1} is suggested. From ground-state ammine models,[31] λ_{ML}^* (resulting from Ru–N bonding changes) is expected to be ~ 500 cm^{-1}. Estimation of λ_o^* is more difficult: The high solvent dependence of E_{op} observed for these complexes is due, to a great extent, to the sensitivity of the E° for the $Ru(NH_3)_5^{3+/2+}$ couple to solvent[5]—that is, E^* shifts with solvent. Thus, in contrast to MMCT transitions in related mixed-valence systems,[32] λ_o^* cannot be directly evaluated from the solvent dependence of E_{op}. From a dielectric continuum model[32,33] λ_o^* should depend on the solvent parameter $(1/D_{op} - 1/D_s)$ where D_{op} and D_s are respectively the optical and static dielectric constants of the solvent. It also depends on the size of the complex, on the distance over which charge transfer occurs, and on the square of the net charge transferred (Δe) (and, in a more detailed model, on the internal dielectric constant of the complex[32,34]). When $Ru(NH_3)_5L^{2+}$ (L = py, pz, etc.) is approximated as a single sphere of radius 4.0 Å and unit charge transfer is assumed to occur over a distance of 3.5 Å, λ_o^* is estimated as 6000 cm^{-1} for water and 4750 cm^{-1} for Me_2SO. When the complex is treated as an ellipsoid[32] somewhat smaller λ_o^* values result—ca. 4000 cm^{-1} for water.[34] These values may be reduced depending on the nature of L because of M–L mixing[23] ($\Delta e < 1$), and for L = pz with Δe taken as 0.8, $\lambda_o^* \geq 2400$ cm^{-1} in water is estimated. Finally, the absorption band shapes (nearly Gaussian[4]) and widths (typically[4,5,10,23] 3000–4000 cm^{-1}) place some constraints on the contribution of λ_{IL}^* and on the total value of λ^*. For L = pz in water $\lambda^* = 3200 \pm 400$ cm^{-1} will be used.[35] Somewhat greater values are suggested for L = py.

In addition to nuclear relaxation of the Franck–Condon states discussed above, intersystem crossing of the initially formed singlet MLCT states to their corresponding triplets must be considered. For the MLCT state of $Ru(bpy)_3^{2+}$ the singlet–triplet splitting Δ_{ST} is ~ 3000 cm^{-1}.[36] Thus for complexes such as $Ru(NH_3)_5pz^{2+}$ the lowest energy MLCT excited states, thermally relaxed triplets,

(30) (a) Kober, E. M.; Meyer, T. J. *Inorg. Chem.* **1984**, *23*, 3877. (b) See: Lumpkin, R. S.; Meyer, T. J. *J. Phys. Chem.* **1986**, *90*, 5307. Also: Kober, E. M.; Caspar, J. V.; Lumpkin, R. S.; Meyer, T. J. *J. Phys. Chem.* **1986**, *90*, 3722 and references cited therein.

(31) See: Gress, M. E.; Creutz, C.; Quicksall, C. O. *Inorg. Chem.* **1981**, *20* 1522 and ref 32 and 33.

(32) Brunschwig, B. S.; Ehrenson, S. E.; Sutin, N. *J. Phys. Chem.* **1986**, *90*, 3657.

(33) See: Sutin, N. *Prog. Inorg. Chem.* **1983**, *30*, 441.

(34) Brunschwig, B. S.; Sutin, N., unpublished work.

(35) (a) If, as assumed here, there are three classes of distortion modes—one classical ($h\nu_o \ll 2kT$), one intermediate ($h\nu_{ML} \sim 2kT$), and one high-frequency ($h\nu_{IL} > 2kT$)—and the absorption (or emission) band is Gaussian-shaped, the full width at half height $\Delta\nu_{1/2}$ is related to the distortions through[35b]

$$\frac{(\Delta\nu_{1/2})^2}{5.55} = \lambda_o^*(2kT) + \lambda_{ML}^*\left(h\nu_{ML} \coth\left(\frac{h\nu_{ML}}{2kT}\right)\right) + \lambda_{IL}^*(h\nu_{IL})$$

Lower and upper limits on λ^* may be obtained from the bandwidth by assuming λ^* to be either entirely λ_{IL}^* or entirely λ_o^*, respectively. (But note that while the second case λ_{ML}^*, $\lambda_{IL}^* = 0$ corresponds to a Gaussian-shaped band, the first with λ_o^*, $\lambda_{ML}^* = 0$ would yield a *line* spectrum not necessarily Gaussian-like in profile.) In this manner, limits $1500 < \lambda^* > 4500$ cm^{-1} are obtained for L = pz in water ($\Delta\nu_{1/2}$ 3200 cm^{-1}; $h\nu_{IL}$ 1300 cm^{-1}).[35c] The lower limit may be refined as follows: The minimum λ^* (which must be dominated by λ_{IL}^*) that is consistent with a structureless band has sufficient broadening from λ_o^* and λ_{ML}^* to "smear" the $h\nu_{IL}$ progression, requiring

$$[5.55(\lambda_o^*(2kT) + \lambda_{ML}^*(h\nu_{ML}) \coth (h\nu_{ML}/2kT))]^{1/2} \sim 1.5h\nu_{IL}$$

Thus the λ_{IL}^* estimate is reduced but λ_o^* and λ_{ML}^* (and λ^*) are increased. Keeping the intermediate frequency contribution constant even within the above constraints, there are a number of λ_o^*, λ_{IL}^* combinations which are consistent with the experimental band shape as ascertained by band-shape simulation.[35d] The λ^* values in the text (2800–3600 cm^{-1}) reflect the range of combinations possible. (b) Ballhausen, C. J. *Molecular Electronic Structures of Transition Metal Complexes*; McGraw-Hill: New York, 1979; Chapter 4. (c) The choice of 1300 = $h\nu_{IL}$ is by analogy with the polypyridine complexes. No structured MLCT absorption (emission) appears to have been reported for complexes of the pyridine family. Ground-state Raman spectra of L = pz and py complexes [Farqharson, S.; Guyer, K. L.; Lay, P. A.; Magnuson, R. H.; Weaver, M. J. *J. Am. Chem. Soc.* **1984**, *106*, 5123] indicate ground-state intraring bands at ~ 650, ~ 1000, ~ 1200, and ~ 1600 cm^{-1} and, in related binuclear complexes [Strekas, T.; Spiro, T. *Inorg. Chem.* **1976**, *15*, 975], all these bands are resonance enhanced upon "MLCT" excitation. Thus all or any of these modes might equally well be used as a basis for the "high-frequency progression". [Actually the vibronic progression will be spaced by excited-state $h\nu_{IL}$. The assumption is that the ground- and excited-state frequencies are similar.] (d) A two-mode (classical + high frequency) model was used; Franck–Condon factors for the high-frequency mode were calculated in the low-temperature limit assuming identical harmonic ground- and excited-state energy surfaces. Contributions from the low-frequency mode were incorporated by broadening each vibronic line with a Gaussian of line half-width LW and the resulting Franck–Condon profile was obtained by summing over all the vibronic transitions. The LW was comprised of 500 cm^{-1} λ_{ML} of $h\nu_{ML} = 400$ cm^{-1} and a variable λ_o contribution, i.e.

$$LW = [5.55(\lambda_o^*(2kT) + \lambda_{ML}^*(h\nu_{ML}) \coth (h\nu_{ML}/2kT))]^{1/2}$$

(36) Felix, F.; Ferguson, J.; Güdel, H. U.; Ludi, A. *J. Am. Chem. Soc.* **1980**, *102*, 4096. Kober, E. M.; Meyer, T. J. *Inorg. Chem.* **1982**, *21*, 3697.

Table IV. MLCT Band Maxima, Excited-State Lifetimes, and Ligand-Loss Quantum Yields for $Ru^{II}(NH_3)_5L$ Complexes in Aqueous Solutions, ~25 °C

L	λ_{max}, nm ($\bar{\nu}_{max}$, $\times 10^3$ cm^{-1})	τ_{MLCT},[a] ps	λ_{exc}, nm	ϕ_L[c]	ϕ_{NH_3}[c]
py	407 (24.6)	$\ll 20$[b]	405	0.045 (2)	0.063 (5)
			449	0.049 (1)	0.063 (1)
4-C_6H_5py	446 (22.4)	~450	405	0.031	0.041
			449	0.033	0.019
pz	472 (21.2)	225	479	0.00014 (1)	0.00018 (2)
		77[h]			
isn	479 (20.9)	140	405	0.004 (1)	0.022 (2)
			479	0.001	0.0053 (2)
			546	0.0003	0.0007
4,4′-bpy	480 (20.8)	<36, 230	254		0.22 (3)[a]
			437	0.0004[f]	
			500		0.007 (5)[a]
4-(ac)py	523 (19.1)	<20	405	0.0045 (7)	0.027 (1)
			449	0.0014 (1)	0.0086 (5)
			520	0.00025 (6)	0.0009 (1)
4,4′-bpyH$^+$	570 (17.5)	<30	560		0.004 (3)[a]
pzH$^+$	529 (18.9)	25[h]	529	0.00011 (2)	
	880 (11.4)[d,e]				
pzR^{3+}[g]	529 (18.9)		437	0.00007[3][f]	
			546	0.00000[3][f]	
pzCH$_3^+$	540 (18.5)	<30	546	0.00004 (1)	0.0005 (2)
	880 (11.4)[d]				
NH_3	390 (25.6)		405		0.27[i]
			313		0.25

[a] This work λ_{exc} = 532 nm unless otherwise noted. [b] λ_{exc} = 355 nm. As shown in Table I this is assumed to give initial MLCT excitation. If the LF absorption spectrum of the py complex is the same as that for $Ru(NH_3)_6^{2+}$, both LF and MLCT excitation should occur at 355 nm.[37] However, if the ligand-field molar absorptivity of $Ru(NH_3)_5py^{2+}$ at 355 nm is comparable to that of $Ru(NH_3)_6^{2+}$, MLCT population predominates with 355-nm excitation because $\epsilon_{MLCT} \sim 3 \times 10^3$ M^{-1} cm^{-1} vs. $\epsilon_{LF} \leq 3 \times 10^1$ M^{-1} cm^{-1} at this wavelength. [c] Reference 1 or 6c unless otherwise noted. [d] This work; cf. ref 15. [e] For the 880-nm band ϵ is ~200 M^{-1} cm^{-1}. [f] Moore, K. J.; Lee, L.; Figard, J. E.; Gelroth, J. A.; Stinson, A. J.; Wohlers, H. D.; Petersen, J. D. *J. Am. Chem. Soc.* **1983**, *105*, 2274. [g] R = $[Rh(NH_3)_5]^{3+}$ which is photoinactive in this complex; the lowest energy band is a shoulder at ~750 nm (J. Wishart, private communication). [h] Reference 2a. [i] The band at 390 nm is the first observed LF transition. Photooxidation to $Ru(NH_3)_6^{3+}$ is also found.[1]

could lie ~6000 ± 1000 cm^{-1} ($\lambda^* + \Delta_{ST}$) below the Franck–Condon excited states observed in absorption measurements, giving lowest MLCT excited-state energies E^* of $\sim 19 \times 10^3$, $\sim 15 \times 10^3$, and $\sim 13 \times 10^3$ cm^{-1} for L = py, pz, and 4-acpy, respectively. Indeed the range of MLCT excited-state energies encompassed by this ligand series is noteworthy. From ν_2 and the above considerations, $E^* \sim 5 \times 10^3$ cm^{-1} (0.6 eV) for the L = pzCH$_3^+$ or pzH$^+$ complex. Thus the series L = pz ... L = pzH$^+$ spans the range $E^* = 19 \times 10^3$ to 5×10^3 cm^{-1}. (Note that E^* for the higher excited state for L = pzCH$_3^+$ is not simply related to that for L = py, etc., or to ν_2 for pzCH$_3^+$ because the intramolecular distortions (IL and ML) are probably greater as a result of the antibonding nature of the state while λ_0^* is much smaller.)

Ligand-Field Excited-State Energies. While the energies of the lowest energy MLCT excited states of $Ru(NH_3)_5L^{2+}$ were discussed above, knowledge of the energies of the ligand-field excited states is also of critical importance to an understanding of the photophysics and photochemistry of this series. LF absorption bands have not been observed for $Ru(NH_3)_5L^{2+}$ when L is of the pyridine family. Presumably the LF bands are masked by the intense MLCT absorptions. For $Ru(NH_3)_6^{2+}$, the $^1A_{1g} \rightarrow {}^1T_{1g}$ and $^1A_{1g} \rightarrow {}^1T_{2g}$ bands are observed at 390 and 310 nm, respectively,[37] but singlet–triplet absorption has not been observed. In order to estimate the properties of the $Ru(NH_3)_6^{2+}$ ligand-field states, we draw on data for other d^6 systems given in Table III. From the spin-allowed ligand-field transitions, B is evaluated as 414 cm^{-1} for $Ru(NH_3)_6^{2+}$. From the "model" systems, the values $C/B = 6.5$ and $C = 2700$ cm^{-1} are inferred, yielding $\Delta_0 = 28\,300$ cm^{-1} and a $\Delta_{ST}(T_1)$ splitting of 5400 cm^{-1} for $Ru(NH_3)_6^{2+}$.[38] To evaluate λ^* and estimate the thexi $^3T_1$ excited-state energy E^* we note that, for the systems in Table III, the relationship $\lambda^* = 4.5 \times 10^{-6} (\Delta_0)^2$ (both λ^* and Δ_0 in cm^{-1}) holds; thus $\lambda^* = 3600 \pm 1000$ cm^{-1} and $E^* = 16\,600 \pm 2000$ cm^{-1} are obtained for the $^3T_1$ state of $Ru(NH_3)_6^{2+}$. (These parameters place the Franck–Condon $^5T_2$ ligand field state at 32 900 cm^{-1}.) The same parameters will be adopted for the $Ru(NH_3)_5L^{2+}$ complexes. These values give a predicted ligand-field emission maximum of 13 000 ± 3000 cm^{-1}—to be compared with the broad emission maximizing at <12 600–11 000 cm^{-1} reported by Cremers for $Ru(NH_3)_5L^{2+}$ (L = py, nic, pz, etc.) at 77 K in crystalline solids.[7]

Photophysical Manifolds for $Ru(NH_3)_5L^{2+}$ Complexes. The excited-state energies inferred above will next be discussed in terms of the ps observations and the (one-photon) photochemistry of the $Ru(NH_3)_5L^{2+}$ complexes. For this purpose, spectral, lifetime, and quantum yield data are summarized in Table IV and a qualitative model of the excited-state manifold is given in Figure 14. The extreme cases, L = py and pzH$^+$—highest and lowest energy MLCT states—are considered first. For these two, despite the considerable uncertainties in λ^* and Δ_{ST} for both LF and MLCT excited states, the relative dispositions of the states are clear. For L = py the lowest triplet LF states are almost certainly lower than the lowest energy MLCT excited state. This assignment, proposed by Ford and co-workers,[6] is consistent with the high photoactivity of $Ru(NH_3)_5py^{2+}$ and the very short-lived MLCT state(s) ($\ll$20 ps): singlet and triplet MLCT are strongly coupled to the lower energy LF states. By contrast, for L = pzH$^+$ the opposite situation—lowest MLCT state much lower in energy than the lowest LF state—obtains. This is consistent with the very low photoactivity of $Ru(NH_3)_5pzH^{3+}$ and $Ru(NH_3)_5(pzCH_3)^{3+}$ *and* the very short MLCT excited-state lifetime: Since E^* for L = pzH$^+$ is only ~5000 cm^{-1}, with λ^* of comparable magnitude, the excited-state to ground-state transition should be in the strongly coupled regime with negligible activation barrier (see Figure 14). This is consistent with the very rapid nonradiative decay rate constant ($>3 \times 10^{10}$ s^{-1}) observed.

For complexes such as $Ru(NH_3)_5pz^{2+}$ and $Ru(NH_3)_5isn^{2+}$ (λ_{max} 470–480 nm), the estimated lowest MLCT excited-state energies (~15 000 cm^{-1}) are close to the estimated equilibrated ^{3}LF energy

(37) Matsubara, T.; Efrima, S.; Metiu, H. I.; Ford, P. C. *J. Chem. Soc., Faraday Trans. 2* 1979, *75*, 390.

(38) (a) The $^1A_{1g} \rightarrow {}^3T_{1g}$ absorption is thus predicted to lie at 500 nm. No peak is found in this region for freshly prepared 0.1 M $Ru(NH_3)_6^{2+}$ solutions. (Over ~1 h a weak 520-nm peak of unknown origin grows in.) Low-temperature studies which may yield better resolved spectra are planned. (b) Note that Bignozzi et al. have estimated $E^* = 1.5 \times 10^4$ cm^{-1} for $Ru(NH_3)_6^{2+}$ (Bignozzi, C. A.; Roffia, S.; Scandola, F. *J. Am. Chem. Soc.* **1985**, *107*, 1644).

Table V. Typical Incident Light Intensities I_{in} and Photon Numbers $N_{h\nu}$ for Flash and Continuous Photolysis Experiments

experiment	I_{in}, einstein cm^{-2} s^{-1}	Δt, s	$N_{h\nu}$, einstein cm^{-2}
450-W Xe lamp[a] vis, 10 min. photolysis	$(0.1-1) \times 10^{-7}$	6×10^{2}	$(0.6-6) \times 10^{-5}$
dye laser, 480 nm[b] Phase R, 0.5-μs pulse	10^{0}	10^{-6}	1×10^{-6}
Q-switched, ν-doubled, Nd laser[c] 532 nm, 20-ns pulse	$10^{0}-10^{2}$	2×10^{-8}	$(0.2-20) \times 10^{-7}$
mode-locked, ν-doubled, Nd laser[d] 532 nm, 30-ps pulse			
"low power" (0.8 mJ/pulse)	7×10^{3}	3×10^{-11}	2×10^{-7}
"high power" (10 mJ/pulse)	1×10^{5}	3×10^{-11}	3×10^{-6}

[a] Typical application: the 5-nm bandwidth 500–600-nm photolysis of $Ru^{II}(NH_3)_5L$ (L = 4,4′-bpy or 4,4′-bpyH$^+$) as described in the Experimental Section. [b] Typical application: Hoselton, M. A.; Lin, C-T.; Swharz, H. A.; Sutin, N. *J. Am. Chem. Soc.* **1978**, *100*, 2383. [c] Typical application: the ns flash photolysis of $Ru(NH_3)_5L^{2+}$ (L = pz, 4,4′-bpy) described in Results; cf.: Creutz, C.; Sutin, N.; Brunschwig, B. S. *J. Am. Chem. Soc.* **1979**, *101*, 1297. [d] This work.

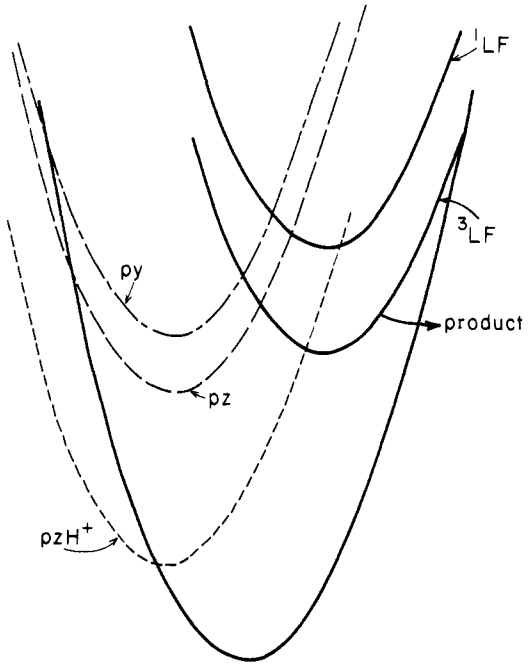

Figure 14. Photophysical manifold for $Ru(NH_3)_5L^{2+}$ complexes. Bottom curve repesents the ground state. Upper states on the left-hand side are MLCT triplets (with both $\lambda^* = 4000$ cm^{-1}, $\Delta_{ST} = 3000$ cm^{-1} assumed constant) for pyridine (py, $\lambda_{max} = 407$ nm), pyrazine (pz, $\lambda_{max} = 470$ nm), and pyrazinium (pzH$^+$, $\lambda_{max} = 880$ nm) complexes. Upper states on the right-hand side are ligand-field states ($\lambda^* = 3600$ cm^{-1}) inferred for $Ru(NH_3)_6^{2+}$. The LF states are assumed to be invariant with L. The crossings of MLCT with LF "surfaces" can only be qualitatively shown (λ^* for MLCT involves intraligand, metal–ligand, and solvent contributions while that for LF arises predominantly from metal–ligand contributions).

(16 600 cm^{-1}), and the energy estimates are not sufficiently reliable to predict a priori which excited state is the lower in energy. The photoaquation yields suggest that ^{3}MLCT is lower—possibly by ~7 kcal mol^{-1} (2500 cm^{-1})—for isn.[6c] If this is the case, the 100–200-ps MLCT excited-state lifetime is determined largely by the MLCT-to-ground-state nonradiative transition (with a small contribution from activated ^{3}MLCT-^{3}LF transition). With the above λ^*(MLCT) and E^* values the MLCT excited-state to ground-state transition is predicted to be weakly coupled ("inverted") and is observed to be at least a factor of 10 slower than that for the strongly coupled L = $pzCH_3^+$ complex.[39]

A striking feature of $Ru(NH_3)_5L^{2+}$ photoactivity is the wavelength dependence of both metal–ligand[6] and intraligand[40] photoreactions. While the polypyridine complexes $Ru(bpy)_3^{2+}$ and $Ru(tpy)_2^{2+}$, etc., are dominated by wavelength-independent lowest excited-state MLCT chemistry,[3] the closely related *cis*-$Ru(bpy)_2L_2^{2+}$ (L = *cis*- or *trans*-stilbazole) does[41] exhibit wavelength-dependent intraligand (π,π^*) or MLCT chemistry. The most studied wavelength-dependent d^6 systems are the cobalt(III) ammines, and excitation-wavelength dependent (or time-dependent) chemistry[6a,42] or emission[43,44] are notable for many low-spin d^6 complexes. For the $Ru(NH_3)_5L^{2+}$ complexes, wavelength-dependent ligand loss, with $\lambda_{exc} \geq 400$ nm, appears to be associated with relaxation of the Franck–Condon MLCT states to *lowest energy* MLCT states. This could arise because internal conversion (e.g., of ^{3}MLCT to ^{3}LF) along metal–ligand modes is competitive in rate with ^{3}MLCT relaxation along (predominantly) solvent and intraligand modes. The "leaking" of unrelaxed MLCT states into the LF manifold could involve nuclear tunneling. The fact that the latter process decreases in probability with (product LF) vibrational level provides a qualitative explanation for the observation[6c] that the log ϕ_{tot} values decrease linearly with irradiation (excitation) energy. (Note that this model for the wavelength dependence requires that reaction from the LF state be competitive in rate with its "back" internal conversion to the MLCT state.) Alternative explanations include direct LF excitation[45a] and "hot" molecule processes.[45b]

Multiphoton Effects. Light intensities characteristic of continuous photolysis and different flash-photolysis experiments are summarized in Table V. In general, the number of incident photons (far right column) determines the magnitude of the signal. Thus, in highly time-resolved experiments (short pulses), high-incident intensities are used to compensate for the short irradiation times. When the number of photons is greater than the number of ground-state molecules, the probability of one-photon excitation is proportional to the (constant) light intensity. The probability of two-photon absorption increases as the square of the light intensity. Consequently, in a given system two-photon processes

(39) The longest lived MLCT state investigated in this study is that with L = 4-phenylpyridine ($\tau \sim 450$ ps). Like the pyridine complex, it manifests[6] wavelength-independent, rather high-yield photoaquation (see Table IV). Yet the MLCT state of the pyridine complex is the shortest lived. The 4-phenylpyridine pattern (high photoactivity and long MLCT lifetime) suggests that the decay of the 4-phenylpyridine MLCT excited state is dominated by relaxation to a (triplet) ligand-field state, in contrast to the pz, isn, etc., MLCT excited states which are dominated by decay to the ground state.

(40) Wagner, P. J.; Bartoszek-Loza, R. *J. Am. Chem. Soc.* **1981**, *103*, 5587.
(41) Zarnegar, P. P.; Whitten, D. G. *J. Am. Chem. Soc.* **1971**, *93*, 3776.
(42) Wrighton, M. S.; Abrahamson, H. B.; Morse, D. L. *J. Am. Chem. Soc.* **1976**, *98*, 4105.
(43) Watts, R. J.; Van Houten, J. *J. Am. Chem. Soc.* **1978**, *100*, 1718.
(44) Servaas, P. C.; van Dijk, H. K.; Snoeck, T. L.; Stufkens, D. J.; Oskam, A. *Inorg. Chem.* **1985**, *24*, 4494.
(45) (a) To account for wavelength-dependent photochemistry, Cremers[7] proposed an inner filter model. The LF state was assumed to be LEES for all L and conversion of MLCT to LF states was assumed to occur. A modified "inner filter model" can be devised to account for wavelength-dependent photochemistry with the LEES being MLCT. The model involves (i) direct excitation into the ligand-field state (with "filtering" by the MLCT absorption) and (ii) LF photochemistry rapid compared to internal conversion/intersystem crossing to the MLCT state when the latter is the LEES. Some direct LF excitation (in addition to, or instead of, nuclear tunneling from the MLCT state) is also a possibility for certain of the systems considered here. (b) A final possibility consistent with the wavelength dependence is "hot molecule" processes—that is, that ligand loss is rapid in comparison with thermal relaxation (of LF or ground states) and that the more vibrationally "hot" the state the higher is its reactivity toward ligand loss.

are ~200 times more probable in "high power" than in "low power" ps experiments and ~10^5 more likely in the latter than in the 20-ns-pulse experiments, etc. Analogous considerations also apply to higher order processes.

As noted earlier, strongly absorbing (uncharacterized) products resulted from the ps 532-nm excitation of $Ru(NH_3)_5L^{2+}$ at "high power". Furthermore anomalously high photoaquation yields were found for L = 4,4′-bpy and 4,4′-bpyH$^+$ even at "low power". By contrast, with $Ru(tpy)_2^{2+}$, no such intensity dependence was observed; the 250-ps MLCT state is populated efficiently and decays cleanly to ground state regardless of excitation intensity. The ground-state absorption spectra of $Ru(NH_3)_5(4,4'\text{-bpy})^{2+}$ and $Ru(tpy)_2^{2+}$ are similar—with intense MLCT bands (λ_{max} 480 and 470 nm, respectively) in the visible and intraligand π,π^* bands in the UV. For both complexes, the lowest excited state is probably MLCT, but with LF states rather close in energy in both cases. There are two notable differences, however: for $Ru(NH_3)_5(4,4'\text{-bpy})^{2+}$ the MLCT excited state absorbs significantly at 532 nm, while $*Ru(tpy)_2^{2+}$ does not, and $Ru(NH_3)_5(4,4'\text{-bpy})^{2+}$ photochemistry is wavelength dependent while that of $Ru(tpy)_2^{2+}$ is not. For $Ru(NH_3)_5(4,4'\text{-bpy})^{2+}$ photoaquation quantum yields range from 0.2 for 254-nm irradiation to <0.02 for >400-nm irradiation (Table IV). Two-photon excitation (532 nm) of either ruthenium(II) complex corresponds energetically to one-photon UV (266 nm) excitation. In the one-photon case, initial population of intraligand π,π^* excited states is most probable, but the higher ligand-field excited states also lie in this region. [For $Ru(NH_3)_5L^{2+}$, by analogy with $Ru(NH_3)_6^{2+}$,[33] population of "$^1T_2$" or "^5T" states is expected.] For $Ru(NH_3)_5(4,4'\text{-bpy})^{2+}$ both 254 nm (single-photon) photochemistry and ps 532-nm "multiphoton"-induced ligand loss are reasonably attributed to population of highly reactive upper ligand-field states.[46] Reaction from these excited states evidently competes very efficiently with relaxation to the (probably) lowest energy MLCT excited state. (Note that when ligand loss is observed in the ps experiment, e.g., Figure 5, it appears to be complete at the end of the pulse.) By contrast, for $Ru(tpy)_2^{2+}$ and $Ru(bpy)_3^{2+}$, etc., relaxation to the lowest energy MLCT state evidently occurs so rapidly and efficiently that both wavelength dependence and "multiphoton artifacts" are absent. Thus the observation of "multiphoton artifacts" for $Ru(NH_3)_5L^{2+}$ appears to be a variation on the theme of wavelength dependent photochemistry in these systems. (With L = 4,4′-bpy the efficiency of multiphoton absorption may be especially great because ϵ_{532} for the MLCT state exceeds that for the ground state, facilitating sequential two-photon absorption.) From these considerations it seems clear that multiphoton "anomalies" in flash-photolysis experiments may, in general, be rather likely for substrates which exhibit wavelength-dependent photochemistry or photophysics.

(46) The high reactivity postulated for the upper ligand-field states must be contrasted to the behavior found for $Rh^{III}(NH_3)_5L$; for the rhodium(III) systems, the same photochemistry is observed for irradiation in either of the spin-allowed ligand-field bands and for bimolecular triplet sensitization.[1a] This contrast in reactivities could be due to the fact that ^5T states lie relatively much higher for Rh(III) than for Ru(II) (Δ_oRh(III) > Δ_oRu(II)).

Concluding Remarks

Picosecond 532-nm excitation of $Ru(NH_3)_5L^{2+}$ complexes yields short-lived (τ <20 to ~200 ps) transients with visible-near-UV spectra consistent with those expected for $Ru^{III}L^{\bullet-}$ species (MLCT states). LF excited states of the complexes are not directly observed and are inferred to be shortlived compared to the MLCT states. With L = 4,4′-bpy and pz, ns flash experiments provide evidence of protonation of the very basic uncoordinated nitrogen in the $Ru(NH_3)_5L^{2+}$ MLCT excited state by solvent water. Spectral analysis, the spectroscopic parameters of related compounds, and data for ground-state systems have been used to estimate the relative orderings of MLCT and LF excited states for the various $Ru(NH_3)_5L^{2+}$ complexes. The estimated energies and transient results are generally consistent with the Ford LEES model; however, the "last word" on these manifolds cannot be said without further detailed spectroscopic studies. An experimentally troublesome feature of these systems—their susceptibility to multiphoton-induced photochemistry—is discussed in terms of their (equally annoying) wavelength dependences.

Acknowledgment. This research was carried out at Brookhaven National Laboratory under contract DE-AC02-76H00016 with the U.S. Department of Energy and supported by its Office of Basic Energy Sciences. We thank Drs. B. Brunschwig, G. Crosby, L. Della Ciana, A. Haim, and J. Wishart for helpful discussions and M. H. Chou for assisting in some of the experiments. We also thank Dr. B. Brunschwig for use of his absorption band simulation program.

Supplementary Material Available: Excitation energy dependence of 470-nm transient absorption changes for $Ru(NH_3)_5(4,4'\text{-bpy})^{2+}$ (Figure S-1) and transient kinetic data for $Ru(NH_3)_5L$ (Figures S-2–S5) [L = protonated pyrazine and 4,4′-bipyridine (Figure S-2), L = pyrazine (Figure S-3), L = isonicotinamide (Figure S-4) and L = pyridine (Figure S-5)] (6 pages). Ordering information is given on any current masthead page.